Published in final edited form as:

Nature. 2017 December 14; 552(7684): 194–199. doi:10.1038/nature25016.

Alcohol-abuse drug disulfiram targets cancer via p97 segregase adapter NPL4

Zdenek Skrott[1,*], **Martin Mistrik**[1,*], **Klaus Kaae Andersen**[2], **Søren Friis**[2], **Dusana Majera**[1], **Jan Gursky**[1], **Tomas Ozdian**[1], **Jirina Bartkova**[2,5], **Zsofia Turi**[1], **Pavel Moudry**[1], **Marianne Kraus**[6], **Martina Michalova**[1], **Jana Vaclavkova**[1], **Petr Dzubak**[1], **Ivo Vrobel**[1], **Pavla Pouckova**[4], **Jindrich Sedlacek**[7], **Andrea Miklovicova**[8], **Anne Kutt**[2], **Jing Li**[3], **Jana Mattova**[4], **Christoph Driessen**[6], **Q. Ping Dou**[9,10], **Jørgen Olsen**[2], **Marian Hajduch**[1], **Boris Cvek**[7,&,#], **Raymond J. Deshaies**[3,11,§,#], and **Jiri Bartek**[2,5,#]

[1]Institute of Molecular and Translational Medicine, Faculty of Medicine and Dentistry, Palacky University, Olomouc, Czech Republic [2]Danish Cancer Society Research Center, DK-2100 Copenhagen, Denmark [3]Division of Biology and Biological Engineering, Caltech, Pasadena, CA 91125, USA [4]Institute of Biophysics and Informatics, First Faculty of Medicine, Charles University, 120 00 Prague 2, Czech Republic [5]Science for Life Laboratory, Division of Genome Biology, Department of Medical Biochemistry and Biophysics, Karolinska Institute, Stockholm, Sweden [6]Kantonsspital St. Gallen, Department Oncology/Hematology, St. Gallen, Switzerland [7]Department of Cell Biology & Genetics, Palacky University, Olomouc, Czech Republic [8]Psychiatric hospital, 785 01 Šternberk, Czech Rep [9]Barbara Ann Karmanos Cancer Institute and Department of Oncology, School of Medicine, Wayne State University, Detroit, MI, USA [10]School of Basic Medical Sciences, Affiliated Tumor Hospital of Guangzhou Medical University, Guangzhou 511436, People's Republic of China [11]Howard Hughes Medical Institute, Caltech, Pasadena, CA 91125, USA

Abstract

[#]*Corresponding Authors: Jiri Bartek* (jb@cancer.dk); *Boris Cvek* (CvekB@seznam.cz), and *Raymond J. Deshaies* (deshaies@caltech.edu).

[§]Present address: Amgen, Thousand Oaks, California 91320, USA

[&]Present address: Olomouc University Social Health Institute, Palacky University, Olomouc, Czech Republic

[*]Equal contribution

AUTHOR CONTRIBUTIONS

Z.S., M. Mistrik, B.C., R.J.D. and J. Bartek conceived the study. Z.S. and M. Mistrik preformed most biochemical and microscopy experiments and wrote the manuscript. D.M. established the expression cell lines and performed most cytotoxicity tests. T.O., P.D. and I.V. performed the HPLC experiments. K.K.A, S.F. and J.O. performed the epidemiological analyses. J. Bartkova performed the immunohistochemical analyses. J.V. and P.D. performed DARTS experiments. P.M. performed cell death analyses. Z.T. performed cytotoxicity tests and heat shock response analyses. A.K. performed cytotoxicity tests. A.M. designed and performed the Antabuse patient's phlebotomies. M. Michalova performed the ITC. J.G. performed FACS analyses, cell death assays, cell sorting. J.S. performed 20S proteasome assays. J.L. performed 26S proteasome assays. M.K. and C.D. performed the cytotoxicity experiments on myeloid and patients derived cell lines. P.P., J.M. and M.H. performed mouse experiments. J. Bartek, B.C., Q.P.D and R.J.D helped design the experiments, interpreted the data and edited/wrote the manuscript. All authors approved the manuscript.

R.J.D. is a founder and consultant for Cleave Biosciences. The remaining authors declare no competing financial interests. Readers are welcome to comment on the online version of the paper.

Cancer incidence is rising and this global challenge is further exacerbated by tumour resistance to available medicines. A promising approach to such unmet need for improved cancer treatment is drug repurposing. Here we highlight the potential for repurposing disulfiram (Antabuse), an old alcohol-aversion drug effective against diverse cancer types in preclinical studies. Our nationwide epidemiological study reveals that patients who continuously used disulfiram have a lower risk of death from cancer compared to those who stopped using the drug at their diagnosis. Moreover, we identify ditiocarb-copper complex as the metabolite of disulfiram responsible for anticancer effects, and provide methods to detect its preferential accumulation in tumours and candidate biomarkers for impact in cells and tissues. Finally, our functional and biophysical analyses reveal the long-sought molecular target of disulfiram's tumour suppressing effects as NPL4, an adapter of p97/VCP segregase essential for protein turnover involved in multiple regulatory and stress-response cellular pathways.

Despite advances in understanding cancer biology, malignant diseases exert an enormous global toll. Furthermore, the increasing average human life expectancy is predicted to bring about demographic consequences including increased incidence of cancer. The high cancer-associated morbidity and mortality highlight the need for innovative treatments. Given the high costs, failure rate, and long testing periods of developing new medicines, repositioning drugs approved for treatment of diverse diseases as candidate anti-cancer therapeutics represents a faster and cheaper alternative[1], benefitting from available clinically suitable formulations and evidence of tolerability in patients. Among promising cancer-killing drugs[2] is disulfiram (tetraethylthiuram disulfide, DSF; Antabuse), used for over 6 decades in treatment of alcohol dependence,[3] with well-established pharmacokinetics, safety and tolerance at FDA-recommended dosage[4]. In the body, DSF is metabolized to diethyldithiocarbamate (ditiocarb, DTC) and other metabolites some of which inhibit liver aldehyde dehydrogenase[5]. As DSF showed anti-cancer activity in preclinical models[3,6–9] and a clinical trial of adjuvant DTC to treat high-risk breast cancer[10], DSF emerges as a candidate for drug repurposing in oncology. Additional advantages of DSF include a broad spectrum of malignancies sensitive to DSF, and its ability to target also the stem-like, tumour initiating cells[11]. While the mechanism of DSF's anti-cancer activity remains unclear, including suggestions that the drug inhibits proteasome activity[6,12], DSF chelates bivalent metals and forms complexes with copper (Cu) which enhances its anti-tumour activity[6,13]. Besides the lack of a well-defined mechanism of action in cancer cells, the main obstacles for DSF repurposing have been: i) uncertainty about the active metabolite(s) of DSF *in vivo*; ii) lack of assays to measure such active derivative(s) in tumours; iii) missing biomarker(s) to monitor the impact of DSF in tumours and tissues; iv) lacking insights into the preferential toxicity towards cancer cells compared to normal tissues; v) absence of a specific molecular target that could explain the potent anti-tumour activity of DSF. Here, we combine experimental approaches and epidemiology to address the important aspects of DSF in relation to cancer, pursuing the goal of repurposing DSF for cancer therapy. We identify the active metabolite of DSF, provide its biological validation and mechanistic insights including discovery of a biologically attractive, and a so-far unsuspected protein as the target for the anti-cancer activity of DSF.

DSF and cancer: epidemiological analyses

The relative paucity of cancer-related clinical trials with DSF[10,14] prompted us to explore whether DSF use might reduce cancer mortality at a population level. Using the Danish nationwide demographic and health registries we estimated hazard ratios (HR) of cancer-specific mortality associated with DSF use among first-time cancer patients during 2000–2013 (see Methods) (Table 1; Extended Data Fig.1a). DSF users were categorized as i) "previous users", i.e. patients prescribed DSF for alcohol dependence only before their cancer diagnosis, and ii) "continuing users", i.e. patients prescribed DSF both before and after the diagnosis. As expected from the deleterious effects of alcohol abuse on cancer risk and prognosis,[15] cancer-specific mortality was higher among previous DSF users than among never users of DSF. Notably, we also found reduced cancer-specific mortality for cancer overall (Table 1), as well as for cancers of the colon, prostate and breast among continuing users compared to previous DSF users (Extended Data Fig.1a). Stratification by clinical stage (Table 1) revealed reduced cancer-specific mortality with continuing use of DSF even among patients with metastatic disease. While not allowing conclusions about causality, these findings supported the hypothesis that DSF may exert anti-cancer effects among patients suffering from common cancers, prompting us to perform pre-clinical analyses.

Anti-tumour activity of DTC-copper complex: CuET

As DSF anti-cancer activity has been suggested to be copper-dependent[6,13] we compared groups of mice injected with the human MDA-MB-231 cancer cells, fed respectively with: i) normal diet; ii) normal diet plus copper gluconate (gluCu); iii) normal diet plus DSF; or iv) normal diet plus DSF and gluCu, and tumour volume was measured over time (Fig.1a and Extended Data Fig.1b,c). Compared to matched controls, tumour volume in DSF- and DSF/gluCu-treated group at 32 days (at DSF doses equivalent to those used by alcoholics) were suppressed by 57% and 77%, respectively ($p=0.0038$ in favour of the DSF/gluCu treatment *vs*. DSF alone). These results substantiate previous *in vitro*[6,11,13] and *in-vivo*[6–9,13,16] studies indicating that DSF is an efficient anti-cancer agent and that copper potentiates its activity. As DSF's reactive metabolite DTC forms complexes with metals, particularly copper,[17] we argued that a DTC-copper complex (CuET) forms *in vivo* (Extended Data Fig.1d), providing the ultimate anti-cancer metabolite. To test this hypothesis, we developed a high-resolution HPLC-MS-based approach to measure CuET in tissues, and readily detected CuET after a single oral dose of DSF (Extended Data Fig.1e,f). Extracts from plasma, liver, brain, and MDA-MB-231 xenografted tumours contained CuET in samples from the mice treated for 5 days with DSF or DSF/gluCu. The CuET levels in plasma and liver were slightly higher after the DSF/gluCu treatment compared to DSF alone. Notably, the CuET levels in the tumour specimens were almost an order of magnitude higher compared to corresponding liver and brain tissues from the same animals (Fig.1b), suggesting preferential accumulation of CuET in tumours. Importantly, we confirmed formation of CuET also in humans undergoing DSF treatment for alcoholism (Fig.1c).

Next, we synthesized CuET and performed comparative cell culture and animal studies. Short-term (24-hour) and long-term (colony formation, CFA) assays consistently showed

higher cytotoxicity of CuET over the primary DSF metabolite DTC in various cancer cell lines (Fig.1d and Extended Data 1g,). The LD_{50} values of CuET in CFA experiments were ≤ 100 nM in 3/3 tested breast cancer cell lines and similar potency was observed among cell lines derived from human lung, colon and prostate tumours (Extended Data Fig. 2a). These data were corroborated by XTT-based 48-hour cytotoxicity tests on a wider panel of cell types (Extended Data Fig.2b). Unexpectedly, only the most sensitive cell lines (e.g. AMO-1, Capan1) showed markers of apoptosis[18] including AnexinV and activated caspases, while in the majority of the cell lines, exemplified by MDA-MB-231 and U-2OS, CuET induced apoptosis-independent cell death (Extended Data Fig.2c–f).

Direct therapeutic effects of CuET *in-vivo* were then documented using the MDA-MB-231 breast cancer (Fig.1e) and AMO-1 myeloma (Fig.1f), xenograft models treated intraperitoneally with a CuET/albumin formulation, thereby confirming antitumor activity and good tolerability of this DSF metabolite (Extended Data 1h,i).

CuET inhibits p97-dependent protein degradation

Next, we interrogated CuET's interplay with cellular protein degradation, one of the suggested explanations for anti-tumour effects of DSF[6,12]. We confirmed that CuET induces phenotypic features shared with proteasome inhibitors such as MG132 or Bortezomib (BTZ), including accumulation of poly-ubiquitylated (poly-Ub) proteins (Fig.2a; Extended Data Fig.3a), rapid deubiquitylation of histone H2A (uH2A)[19] (Extended Data Fig.3b), and accumulation of ubiquitylated proteins in the cytoplasm (Extended Data Fig.3c)[19]. Furthermore, TNFα-induced degradation of IκBα[20] was blocked after 1-hour treatment with CuET or BTZ (Fig.2b). Finally, CuET inhibited degradation of Ub-(G76V)-GFP (Ubiquitin fusion degradation substrate)[21] in a dose-dependent manner (Fig.2c). However, despite these data confirmed a defect in protein degradation, CuET had no effect on the CT-like, C-like or T-like activity of 20S proteasome[22] (Extended Data Fig.3d,e). This notion was further corroborated by the lack of stabilizing effect of CuET on p53 tumour suppressor protein in dicoumarol-treated cells, where p53 turnover depends on the core 20S proteasome independently of ubiquitin[23,24]. Contrary to CuET, treatment with the 20S proteasome inhibitor BTZ stabilized p53 irrespective of dicoumarol (Extended Data Fig.3f), indicating that 20S proteasome-dependent protein turnover remains operational under CuET treatment. Furthermore, CuET failed to inhibit 26S proteasome activity (Extended Data Fig.3g) deduced from Rpn11-dependent deubiquitylation.[25] Collectively, these results suggested that CuET stabilizes ubiquitylated proteins by blocking a step upstream of the proteasome.

Next we considered p97/VCP-dependent processing of poly-Ub-proteins since this pathway operates upstream of the proteasome and its malfunction resembles phenotypes of proteasome inhibition[26]. Unlike BTZ or MG132, CuET induced only modest accumulation (a small subfraction) of HIF1α (Fig.2d), consistently with reported modest accumulation of HIF1α after knock-down of p97 compared to cells with inhibited proteasome[27]. Next, we pre-treated cells with MG132, followed by wash-off and 1-hour cycloheximide (CHX) (inhibitor of translation) treatment combined with BTZ, CuET or DBeQ (direct inhibitor of p97 ATPase activity)[28]. All tested inhibitors prevented degradation of Cdc25A (a known p97-target)[29] while degradation of the largely p97-independent target (the bulk of HIF1α)[27]

was inhibited only by BTZ (Fig.2e). Furthermore, consistent with cleavage of the 120 kDa species of the endoplasmic reticulum (ER)-tethered transcription factor Nrf1 into an active 110-kDa form being a p97-dependent process[30], appearance of the cleaved Nrf1 was inhibited by both CuET and NMS873 (another p97-ATPase inhibitor) (Fig.2f and Extended Data Fig.4a,b). These results suggest that the p97 pathway is compromised in cells treated with CuET.

Next, we asked whether CuET impairs the p97 segregase activity that extracts poly-Ub-proteins from cellular structures such as ER, Golgi apparatus or chromatin for subsequent proteasomal degradation[31]. Using fluorescence recovery after photobleaching (FRAP) to explore the mobility of accumulated poly-Ub-proteins, we found that whereas GFP-Ubiquitin in DMSO- or BTZ-treated cells diffused rapidly into bleached areas, such diffusion was slower upon treatment with CuET or NMS873 (Fig.2g and Extended Data 4c). This suggested that after treatment with CuET or NMS873 at least a subset of the accumulated poly-Ub-proteins remains immobile, likely embedded into cellular structures. Consistently, upon detergent pre-extraction of mobile proteins, we observed greater immunofluorescence signals of extraction-resistant K48-poly-Ub proteins (destined for proteasomal degradation) in NMS873- and CuET-treated cells compared to BTZ- or DMSO-treated controls (Extended Data Fig.4d). Western blot (WB) analysis of ER-rich microsomal fractions also revealed enrichment of poly-Ub-proteins after CuET and NMS873 treatment (Extended Data Fig.4e). Malfunction of p97 segregase is furthermore associated with a cellular unfolded protein response (UPR)[32]. We confirmed UPR in cells treated with CuET or NMS873 by detecting elevated markers of UPR induction including the spliced form of XBP1s protein, ATF4 and p-eIF2-alpha[33] (Extended Data Fig.4f).

Of clinical relevance, inhibition of p97 was suggested as an alternative treatment strategy for myeloma patients who relapsed after therapy with BTZ (Velcade)[34] or Carfilzomib (CFZ)[35]. Thus, we performed cytotoxicity tests with CuET on a panel of BTZ/CFZ-adapted and non-adapted human cell lines derived from myeloma patients treated with Velcade or induced experimentally. All pairs of adapted and non-adapted cells showed similar sensitivity towards CuET treatment, in contrast to BTZ (Extended Data Fig.5a–d). These results suggest that treatment with DSF (best combined with copper) or CuET might become a feasible therapeutic option for patients with relapsed, Velcade-resistant multiple myeloma.

CuET binds and immobilizes NPL4

To elucidate the p97 pathway inhibition by CuET, we first employed an assay for p97 ATPase activity.[28] Unlike NMS873, however, CuET had no effect (Extended Data Fig.6a). As NPL4 and UFD1 proteins represent key components of p97 segregase,[31] we examined whether CuET might target the pathway through these cofactors. Ectopic overexpression of NPL4-GFP, but neither UFD1-GFP nor p97-GFP, dampened CuET cytotoxicity, suggesting NPL4 as the candidate target of CuET (Fig.3a; Extended Data Fig.6b). An analogous ‘rescue effect’ of ectopic NPL4-GFP was apparent from the reduced poly-Ub-protein accumulation caused by CuET (Extended Data Fig.6c).

In live-cell imaging, 2–3-hour exposure to CuET induced prominent nuclear clustering of NPL4-GFP, but not UFD1-GFP or p97-GFP (Fig.3b). Within 2–3 hours, the bulk of cellular NPL4-GFP became immobilized in nuclear clusters and also in cytoplasmic areas as manifested by FRAP (Fig.3c). CuET-induced immobilization of endogenous NPL4 was confirmed by WB-detectable accumulation in detergent-insoluble fractions from various cell lines (Fig.3d) and by immunofluorescence on pre-extracted cells (Extended Data Fig.6d). Importantly, the immobilization of NPL4 was detectable also in pre-extracted sections of cryopreserved tumours from mice treated with DSF or DSF/gluCu, thereby providing a potential biomarker of CuET activity towards the p97 pathway *in-vivo* (Fig.3e).

NPL4 is an attractive candidate for CuET binding because this protein contains two zinc-finger domains: C-terminal NZF (NPL4-zinc-finger) and putative zf-NPL4, respectively,[36] which bind bi-valent metals and metal complexes that might chemically resemble CuET[37]. Using isothermal calorimetry analysis (ITC),[38] we observed a standard dose-response dependent binding curve (Fig 3f) compatible with one binding site for CuET on WT-NPL4, and a K_d in nanomolar concentrations for the NPL4-CuET interaction. Next, we employed mutagenesis to test any role of the putative zf-NPL4 in potential NPL4-CuET interaction. The putative ZF was preferred because an endogenous larger form of NPL4 that exists in human cells, detectable as an upper band on WB (Fig.3d) (with C-terminal NZF substituted by a non-ZF sequence), is still immobilized upon CuET treatment, suggesting the C-terminal NZF is dispensable for CuET interaction. No ITC interaction was found with the mutated NPL4 (MUT-NPL4) (Extended Data Fig.6f) in which both histidines and both cysteines in the putative ZF domain were substituted by alanines (Exteneded Data Fig.6e). As another, independent approach we used Drug Affinity Responsive Target Stability (DARTS), based on altered protease susceptibility of target proteins upon drug binding.[39] Consistently, exposure to CuET caused a differential pronase-dependent proteolysis pattern of WT-NPL4 but not the MUT-NPL4 (Extended Data Fig.6g). These results indicate that NPL4 is directly targeted by CuET and intact NPL4's putative ZF domain is essential for such interaction.

Strikingly, ectopically expressed MUT-NPL4-GFP formed immobile nuclear clusters spontaneously in untreated cells, reminiscent of events seen in cells upon CuET treatment (Fig.3c,g). Moreover, unlike ectopic WT-NPL4, ectopically expressed MUT-NPL4-GFP not only did not render cells resistant towards CuET but it was toxic to the acceptor cells (Extended Data Fig. 6h). We also confirmed that multiple CuET-induced cellular phenotypes were mimicked by the ectopic MUT-NPL4-GFP model, including accumulation of poly-Ub-proteins and UPR activation (Extended Data Fig.6i) and more (see below).

NPL4 forms aggregates triggering heat-shock response

Despite the nuclear NPL4 clusters occupy DAPI-unlabelled areas of chromatin (Extended Data Fig.6d) co-localizations with DAPI-excluded structures: nucleoli and nuclear speckles were not found (Extended Data Fig. 7a). In late-G2 cells NPL4 clusters were evidently excluded from the partially condensed chromatin (Extended Data Fig. 7b), suggesting that the NPL4 aggregates exclude chromatin rather than accumulating in specific nuclear areas. Both the nuclear clusters and the immobilized cytoplasmic NPL4 co-localized with poly-Ub-proteins (confirmed by anti-K48-Ub and FK2 antibodies), small ubiquitin-like modifiers

(SUMOs) (only in nuclei), and with TDP43 protein[40] (Fig.4a and Extended Fig. 7d), all features typical for aggregated defective proteins.[41] The same co-localization patterns were observed for the spontaneous clusters formed by MUT-NPL4-GFP documenting that NPL4 aggregation is sufficient to evoke these phenotypes even without CuET (Extended Data Fig. 7c,e). Blockade of cellular ubiquitylations with a chemical inhibitor (MLN7243) of the E1 ubiquitin-activating enzyme failed to prevent either NPL4-GFP nuclear aggregation or cytoplasmic immobilization (Extended Data Fig. 7d), excluding the immobilization of NPL4 *via* recognition of ubiquitylated/SUMOylated substrates and rather suggesting that immobilized NPL4 attracts ubiquitylated proteins or proteins that subsequently become ubiquitylated/SUMOylated. A key protein commonly associated with intracellular protein aggregates is HSP70, a chaperone implicated in aggregate processing.[42] Indeed, pre-extracted cells showed co-localization of HSP70 with both CuET-induced WT-NPL4-GFP and spontaneous MUT-NPL4-GFP aggregates (Fig. 4b,c). Both the CuET-induced NPL4 aggregates and spontaneous MUT-NPL4 aggregates also co-localized with p97 (Extended Data Fig. 7f,g), as particularly evident after pre-extraction. In the NPL4-GFP model the amount of p97 immunoreactivity within the NPL4-GFP clusters correlated with the GFP signal intensity suggesting that p97 is immobilized *via* its interaction with NPL4. The other NPL4 binding partner, UFD1, was virtually undetectable in detergent-insoluble pellets of CuET-treated or MUT-NPL4-GFP-expressing cells despite obvious p97 immobilization (Extended Data Fig.8a,b), suggesting that UFD1 cannot bind to, or becomes only loosely attached to aggregated NPL4/p97 complex. Importantly, non-extractable cellular p97 is detectable after CuET treatment (Extended Data Fig.8c), including on tumour sections from mice treated with DSF or DSF/gluCu providing an additional candidate marker of CuET activity *in vivo* (Extended Data Fig.8d).

As aggregation of misfolded/damaged proteins triggers cellular heat shock response (HSR) via an HSF1-dependent mechanism,[43] we confirmed that CuET treatment indeed triggered a robust HSR accompanied by characteristic HSF1 nuclear stress foci (Fig.4d) which were also detectable in cells spontaneously aggregating MUT-NPL4-GFP (Fig.4e). HSR markers including accumulation of heat shock proteins and a phosphorylation shift of HSF1 were detectable by WB (Extended Data Fig. 8e,f).

Discussion

This study sheds light on the so far enigmatic anti-cancer activity of the alcohol-abuse drug disulfiram. We propose a model for DSF cytotoxic activity, featuring rapid conversion of DSF into CuET which accumulates in tumours. After entering cells CuET binds NPL4 and induces its aggregation, consequently disabling the vital p97-NPL4-UFD1 pathway and inducing a complex cellular phenotype leading to cell death (Fig. 4f). Supporting CuET as the active metabolite is the correlation of CuET concentrations (active to nanomolar range) with the biological effects and functional impact on the targeted pathway(s) *in-vivo*. Also, as CuET is the only known metabolite of DSF containing copper, a metal that enhances the anti-tumour effects of DSF, it is unlikely that another DSF metabolite could represent the major anti-cancer agent as levels of non-CuET metabolites should be lowered by copper addition. We also present a method for CuET detection in tissues and plasma, and data suggesting that preferential accumulation of CuET in tumours may contribute to cancer cell

toxicity, consistent with the high therapeutic tolerability of DSF,[3] as documented even after years of daily administration at doses comparable with those we used in our mouse experiments. Considering the numerous studies on DSF and diverse opinions about the potential target of its anti-cancer effects,[44] identification of NPL4, a key component of the p97(VCP)-NPL4-UFD1 segregase complex as the molecular target of CuET is surprising. The CuET-NPL4 interaction leads to rapid formation of protein aggregates and immobilization of this otherwise very mobile multifunctional protein complex resulting in a severe phenotype, induction of HSR and eventually cell death. While additional potential targets of CuET cannot be excluded, the malfunction of the p97 pathway due to the NPL4-p97 aggregate formation explains major cell phenotypes and cell death as a consequence. Our work also reconciles the controversial studies[6,12] suggesting proteasome as the DSF target, by demonstrating that neither 20S nor 26S proteasome, but the processing of ubiquitylated proteins by the NPL4-dependent segregase is targeted by CuET. Our results support the notion that the p97/NPL4 pathway is a promising therapeutic target in oncology[45,46]. Indeed, reports on p97 overabundance correlating with progression and metastasis of carcinomas of the breast, colon, and prostate[47–49] are consistent with our present nationwide epidemiological analysis revealing an association between continued use of DSF and favourable prognosis, an intriguing finding worthy of further investigation, particularly given the currently limited therapeutic options for patients with metastatic cancer. From a broader perspective, our study illustrates the potential of multifaceted approaches to drug repositioning, providing novel mechanistic insights, identification of new cancer-relevant targets and inspiration for clinical trials, here with DSF, an old, safe and public domain drug[4] that might help save lives of cancer patients worldwide.

METHODS

Epidemiological analyses and access to health registers

We conducted a population-based cohort study by combining Danish nationwide demographic and health registers. This study was approved by the Danish Data Protection Agency and Statistics Denmark's Scientific Board. As the epidemiological study was based solely on register data and did not involve any contact with patients, no ethical approval was required from the Danish Scientific Ethical Committee[50]. The cohort consisted of all Danes aged 35–85 years with a first-time diagnosis of cancer between January 2000 and December 2013. As disulfiram (DSF; Antabuse) is a relative contraindication among individuals with liver or kidney diseases, we excluded patients with cancers of the liver or kidney from the cohort. Cohort members were categorized according to use of DSF into two main groups: i) those who filled at least one prescription of DSF within five years prior to the cancer diagnosis, but did not fill DSF prescription(s) during the first year after the diagnosis ('previous users'), i.e., generally defining individuals suffering from alcoholism but taking DSF only before their cancer diagnosis, and ii) those who used DSF prior to their cancer diagnosis and also filled one or more DSF prescriptions during the first year after the cancer diagnosis ('continuing users'), i.e., defining individuals who underwent DSF therapy both before and after the cancer diagnosis. We also defined category of cancer patients who did not fill prescription(s) for DSF either before or after (≤1 year) the cancer diagnosis ('never users'). In the main analyses, we calculated hazard ratios (HRs) and 95% confidence

intervals (CIs) estimating cancer-specific mortality among continuing DSF users compared to previous DSF users based on a Cox model regressing on both propensity scores and disulfiram use. By including propensity scores in the regression, we have used demographic data and comorbid conditions/diagnostic codes as well as prescription data for selected concomitant drugs, to balance baseline characteristics of 'previous' and 'continuing' users of DSF and to adjust estimated hazard ratios of cancer-specific mortality associated with DSF use[51]. The cancer patients were followed from one year after the diagnosis until death, migration or end of study (December 31, 2014). The propensity scores thus estimate the probability of being treated with DSF in the exposure window 0–1 year after the cancer diagnoses conditional on the following other covariates in the calculation of propensity scores using logistic regression: gender, age at diagnosis, calendar time, highest achieved education, and disposable income; medical histories of diabetes mellitus, chronic obstructive pulmonary disease, ischaemic heart disease, congestive heart failure, cerebrovascular disease, atrial fibrillation or atrial flutter, dementia, and ulcer disease; and use of non-steroidal anti-inflammatory drugs (NSAIDs; including aspirin), non-aspirin antithrombotic agents (anticoagulants), statins, antihypertensives, other cardiovascular drugs, anti-diabetics, and psychotropic drugs. In the Cox model, the propensity score is further included as a restricted cubic spline to model possible non-linearity's, in addition to the categorical disulfiram use, which is the variable of main interest. Analyses were run for cancer overall and for breast, prostate and colon cancer, separately. Furthermore, all analyses were stratified by stage (localized, non-localized or unknown). Statistical significance of DSF use was evaluated by likelihood ratio tests. We used the software R for statistical computing[52].

In vivo tumour experiments

Human breast cancer cell line MDA-MB-231 was injected (10^7 cells transplanted s.c.) to grow tumours in athymic nu/nu female mice (AnLab Ltd.) of body weight 23,6 – 26,9 g, age of 12 weeks. Inclusion criteria were: female, appropriate age and weight (15–30 g). Exclusion criteria were: tumour size must not exceed 20 mm (volume 4000 mm3) in any direction in an adult mouse, the tumour mass should not proceed to the point where it significantly interferes with normal bodily functions, or causes pain or distress due to its location, persistent self-induced trauma, rapid or progressive weight loss more than 25%, for 7 days. In none of the experiments were these approved ethical limits exceeded. After the tumours grew to 0.114–0.117 cm^3 on average, mice were randomly divided into four groups, each of 8 mice, and treated as follows: 1. normal diet, 2. normal diet plus p.o. 0.15 mg/kg copper gluconate, 3. normal diet plus p.o. 50 mg/kg disulfiram (DSF), 4. normal diet plus p.o. 0.15 mg/kg copper gluconate plus p.o. 50 mg/kg DSF. Administration of compounds was carried out as a blinded experiment (all information about the expected outputs and the nature of used compounds were kept from the animal-technicians). Copper gluconate was administered each day morning (8 am) and DSF each day evening (7 pm) to mimic a clinical trial combining DSF and copper gluconate in treatment of tumours involving liver (NCT00742911). After treatment began, mice were weighed and their tumours measured twice per week. At day 32, mice were sacrificed, tumours taken out and frozen at −80°C. The experiment was evaluated based on comparing growth curves of tumours in the experimental groups with those in controls. The rates of tumour growth inhibition (TGI) were calculated by formula $TGI = (1 – V_{treated}/V_{control}$ where $V_{treated}$ is mean tumour

volumes in treated group and $V_{control}$ is mean of tumour volumes in control group). Mean tumour volume values in specific time intervals were statistically evaluated. To test directly effect of CuET we used MDA-MB-231 and AMO-1 models. MDA-MB-231 was injected (5×10^6 cells were transplanted s.c.) to grow tumours in SCID mice (ENVIGO, NL) age of 10 weeks (+/− 2 weeks). AMO-1 xenografts were expanded in SCID mice. Each group consisted of 10 animals, each bearing two tumours. CuET was formulated in bovine serum albumin solution (1%) to final concentration 1 mg/ml. CuET was applied intraperitoneally in a schedule 5 days ON and 2 days OFF. All aspects of the animal study met the accepted criteria for the care and experimental use of laboratory animals, and protocols were approved by the Animal Research Committee of the 1st Faculty of Medicine Charles University in Prague and Ethical Committee of Faculty of Medicine and Dentistry, Palacky University in Olomouc. For HPLC/MS and IHC analysis we used MDA-MB-231 xenografted mice treated by the same DSF and DSF plus copper gluconate regime as described for the anticancer activity assessment with the important difference that mice were sacrificed already after 5 days of treatment.

HPLC/MS analysis of copper-dithiocarbamate complex (CuET)

The HR-MRM analysis was performed on HPLC-ESI-QTOF system consisting of HPLC chromatograph Thermo UltiMate 3000 with AB Sciex TripleTOF 5600+ mass spectrometer, using the DuoSpray ESI source operated at ion source voltage 5500 V, ion source gas flow rates 40 units, curtain gas flow rate 30 units, declustering potential 100 V and temperature 400°C. Data were acquired in Product ion mode with two parent masses 358.9 and 360.9 for analysis of CuET. Chromatographic separation was done by PTFE column especially designed for analysis of strong metal chelators filled by C18 sorbent (IntellMed, cat.no.IM_301). Analysis was performed at room temperature and flow rate 1500 μL/min with isocratic chromatography. Mobile phase consisted of HPLC grade acetone (Lachner) 99.9%, HPLC water (Merck Millipore) 0.1% and 0.03% HPLC formic acid (Sigma). Acquired mass spectra were evaluated in software PeakView 1.2, where extracted ion chromatograms of transitions 88.0 and 116.0 (common for both parent masses) with 0.1 mass tolerance was Gaussian smoothened with width of 2 points. Peak area was then recorded and recalculated to ng/ml according to calibration curve.

Sample preparation for HPLC/MS analysis

Liquid nitrogen-frozen biological samples were cut into small pieces by scalpel. Sample (30-100 mg) was immediately processed by homogenization in 100% acetone in ratio 1:10 sample vs. acetone (for plasma or serum the ratio was 1:4). Homogenization was done in a table homogenizer (Retsch MM301) placed in a cold room (4°C) in 2 ml Eppendorf tube with 2 glass balls (5mm) for 1min, 30Hz. Next, tube was immediately centrifuged at 4°C, 20.000G, 2min. Supernatant was decanted into a new 1,5 ml Eppendorf tube and immediately centrifuged for 30min using small table centrifuge (BioSan FVL-2400N) placed inside a −80°C freezer. Supernatant was quickly decanted into glass HPLC vial and kept at −80°C not longer than 6 hours. Just before the HPLC analysis the vial was placed into the pre-cooled (4°C) LC-sample rack and immediately analyzed. To enable approximate quantification of analyzed CuET, calibration curve was prepared. Various amounts of CuET were spiked to plasma, frozen in liquid nitrogen, and placed at −80°C to exactly mimic

sample processing. Standards were then processed similarly as the samples described above. To measure circulating CuET concentrations, mice were dosed with single per oral DSF (50 mg/kg) and sacrificed at different time points. Serum was collected and frozen for analysis.

Blood collection from humans for HPLC/MS analysis of CuET

Blood samples were collected before and 3 hours after per oral application of the DSF (Antabuse 400 mg) dissolved in water. Phlebotomy needles were of special type for metal analysis - Sarstedt Safety Kanule 21G × 1½″ REF 85.1162.600. Collection tubes were of special type for metal analysis - Sarstedt – S-Monovette 7,5 ml LH, REF 01.1604.400. Immediately after the blood collection the samples were centrifuged in a pre-cooled centrifuge (4°C at 1300G for 10min). After the spinning, tubes were placed on ice and the plasma fraction was immediately aliquoted into the 1,5-ml Eppendorf tubes with approx. 500ul per tube. The tubes with plasma were immediately frozen on dry ice and later stored in −80°C. Blood samples were collected from volunteers who signed the informed consent and were undergoing Antabuse therapy due to alcohol abuse. Human participants were 4 males (ages 34, 38, 41, 60 years) and 5 females (ages 37, 56, 46, 59, 63 years). All individuals were freshly diagnosed for alcohol use disorder and were scheduled for Antabuse therapy. Blood samples were collected before and after the first application of Antabuse. All relevant ethical regulations were followed for the study. The study including the collection of blood samples was approved by the Ethical Committee of Faculty of Medicine and Dentistry, Palacky University in Olomouc.

Cell lines

Cell lines were cultured in appropriate growth media supplemented with 10% fetal bovine serum and penicillin/streptomycin; and maintained at humidified, 5% CO2 atmosphere at 37°C. Lines cultured in DMEM medium were: HCT116 (ATCC), DU145 (ECACC), PC3 (ECACC), T47D (NCI60), HS578T (NCI60), MCF7 (ECACC), MDA-MB-231 (ATCC), U-2OS (ECACC), HeLa (ATCC), NIH-3T3 (ATCC), CAPAN-1 (ATCC), A253 (ATCC), FaDu (ATCC),, h-TERT-RPE1 (ATCC), HeLa-Ub(G76V)-GFP-ODD-Luc[21]. Cell lines cultured in RPMI1640 medium were: NCI-H358 (ATCC), NCI-H52 (ATCC), HCT-15 (ATCC), AMO-1 (ATCC), MM-1S (ATCC), ARH77 (ATCC), RPMI8226 (ATCC), OVCAR-3 (NCI60), CCRF-CEM (ATCC), K562 (ATCC), 786-0 (NCI60). Cell lines cultured in EMEM medium were: U87-MG (ATCC), SiHA (ATCC). Cell line A549 (ATCC) was cultured in F12K medium, HT29 (ATCC) in McCoy's medium, and LAPC4 (kindly provided by prof. Zoran Culig, University of Innsbruck) in IMDM medium supplemented with metribolone R1881 (Sigma). RWPE-1 (ATCC) cells were cultured in a keratinocyte serum-free medium supplemented with the bovine pituitary extract and human recombinant epidermal growth factor (Thermo Scientific). Bortezomib and carfilzomib resistant multiple myeloma cell lines were previously described in[35]. Cell lines were tested for mycoplasma contamination and authenticated by STR method. None of the cell lines used in this study is listed in the database of commonly misidentified cell lines maintained by ICLAC.

Stable cell lines construction

For construction of all stably transfected cell lines we used the U-2OS cell line (ECACC). For U-2OS-Ub-GFP we used the commercial Ub-GFP EGFP-C1 vector (Addgene), for

U-2OS-NPL4-GFP we used the commercial NPLOC4-GFP pCMV6-AC-GFP vector (Origene), for U-2OS-p97-GFP we used the commercial VCP-GFP pCMV6-AC-GFP vector (Origene) and for U-2OS-UFD1-GFP we used the commercial UFD1L-GFP pCMV6-AC-GFP vector (Origene). Cells were transfected using Promega FugeneHD according to manufacturer's instructions. Cells were further cultivated in the appropriate antibiotics (geneticin, 400 μg/ml). Medium with geneticin was replaced every 2–3 days until the population of resistant cells was fully established. Cells were further refined by sorting for cells expressing GFP signal (BD FACS Aria). For preparation of inducible MUT-NPL4-GFP cells, U-2OS cells were transfected with pcDNA6/TR plasmid (Invitrogen, V1025-20) using FugeneHD transfection reagent (Promega, E2311) according to manufacturer's protocol. To generate a cell line that stably expresses the Tet repressor, U-2OS cells were cultured in selective medium with blasticidin (10 μg/ml) for 10 days. Blasticidin-resistant colonies were picked, expanded and screened for clones that exhibit the lowest basal levels and highest inducible levels of expression. Next, the most suitable clones were transfected with the PCDNA4/TO expression vector encoding the mutated NPL4-GFP protein using the Fugene transfection reagent. Cells were cultured in medium with Zeocin (500 μg/ml) to select clones that contain pcDNA 4/TO-mutated NPL4-GFP. The MUT-NPL4-GFP-encoding plasmid was obtained from GeneriBiotech. To induce expression of protein, cells were incubated with doxycycline (Sigma) 1 μg/ml for 16-48 hours.

Colony formation assay

Cells were seeded into 6-well plates at 100–300 cells per well (depending on the cell line). Next day the cells were treated with compounds as indicated in the specific experiments and kept in culture for 7–14 days. Colonies were visualized by crystal violet and counted.

XTT assay

10.000 cells were seeded into a 96-well plate. Next day, the cells were treated as indicated. After 24 hours an XTT assay was performed according to manufacturer's instructions (Applichem). XTT solution was added to media and incubated for 30–60 minutes, and then dye intensity was measured at the 475nm wavelength using spectrometer (TECAN, Infinite M200PRO). Results are shown as mean values and standard deviations from 3 independent experiments, each performed in 3 replicates. For LD50 analysis across the panel of cell lines listed in Extended data Fig. 2b, cell lines were treated with various doses (at least 5 doses) for 48 hours. LD50s are calculated using Graphpad Prism software based on survival curves from at least two independent experiments.

Annexin V staining

Cell cultures were treated as indicated and harvested by trypsinization. Initial culture medium and washing buffer were collected to include detached cells. Cells were centrifuged (250G, 5min) and re-suspended in a staining buffer (140 mM NaCl, 4 mM KCl, 0.75 mM $MgCl_2$, 10 mM HEPES) containing 2.5 mM $CaCl_2$, Annexin V-APC (1:20, BD Biosciences) and 2.5 μg/ml 7-AAD (BD Biosciences) for 15 minutes on ice in the dark. Samples were analysed by flow cytometry using BD FACSVerse (BD Biosciences), at least 10.000 events were acquired per sample. Collected data were processed by BD FACSSuite (BD Biosciences) and exported into Microsoft Excel.

Caspases 3/7 assay

Activity of caspase-3 and -7 was quantified by cleavage of fluorogenic substrate CellEvent™ Caspase-3/7 Green Detection Reagent (ThermoFisher Scientific). Briefly, samples prepared in the same staining buffer as described for Annexin V staining above were supplemented with 2% FBS, 0.5 μM CellEvent™ Caspase-3/7 Green Detection Reagent and incubated for 45 minutes at room temperature in the dark. Subsequently, 0.5 μg/mL DAPI was added and samples were analysed by flow cytometry using BD FACSVerse (BD Biosciences), at least 10.000 events were acquired per sample. Collected data were processed by BD FACSSuite (BD Biosciences) and exported into Microsoft Excel.

Viability assay of multiple myeloma cells

The CellTiter 96® MTS-assay (Promega) was used to determine the cell viability of bortezomib, (BTZ, obtained from Janssen Cilag), carfilzomib and CuEt in cell lines, according to manufacturer's instructions, and the absorbance of the formazan product was measured in 96 well microplates at 492nm. The assay measures dehydrogenase enzyme activity found in metabolically active cells.

For patient cells, the more sensitive luminescent CellTiter-Glo assay (Promega) was used to determine cell viability, measured by ATP production of metabolically active cells. The primary myeloma cell samples were obtained after written informed consent and approval by the independent ethics review board (St. Gallen ethics committee - Ethikkommission Ostschweiz), in accordance with ICH-GCP and local regulations. Malignant plasma cells were retrieved by PBMC isolation from a patient with multiple myeloma progressing under BTZ containing therapy, based on IMWG criteria ("bortezomib resistant") and an untreated patient ("bortezomib sensitive"). The purity of the cell samples was >80 % myeloma cells, as assessed by morphology.

Immunoblotting and antibodies

Equal amounts of cell lysates were separated by SDS-PAGE on hand-cast or precast tris-glycine gradient (4–20%) gels (Life Technologies), and then transferred onto nitrocellulose membrane. The membrane was blocked with 5% bovine milk in Tris-buffered saline containing 0.1% Tween 20 for 1hour at room temperature, and then incubated overnight at 4°C or 1hour at room temperature, with one of the following primary antibodies (all antibodies were used in the system under study (assay and species) according to the profile of manufacturer): anti-ubiquitin (1:1000; Cell Signaling, cat.n.:3933), anti-H2A, acidic patch (1:1000; Merck Millipore, cat. n.: 07-146), anti-monoubiquityl-H2A (1:1000; Merck Millipore, clone E6C5), anti-IκBα (1:500; Santa Cruz Biotechnology, cat. n.: sc-371), anti-p53 (1:500; Santa Cruz Biotechnology, clone DO-1), anti-HIF1α (1:1000; BD Biosciences, cat. n.: 610958), anti-Cdc25A (1:500; Santa Cruz Biotechnology, clone DCS-120), anti-NRF1 (1:1000, Cell Signaling, clone D5B10), anti-VCP (1:2000; Abcam, cat. n.: ab11433), anti-VCP (1:1000; Novus Bio, cat. n.: NBP100-1557), anti-NPLOC4 (1:1000; Novus Bio, cat. n.: NBP1-82166), anti-ubiquitin lys48-specific (1:1000; Merck Millipore, clone Apu2), anti-β-actin (1:2000; Santa Cruz Biotechnology, cat. n.: sc-1616; or 1:500, Santa Cruz Biotechnology, cat. n. sc-87778), anti-GAPDH (1:1000,GeneTex, clone 1D4), anti-Lamin B (1:1000; Santa Cruz Biotechnology, cat. n.: sc-6217), anti-calnexin (1:500; Santa Cruz

Biotechnology, cat. n.: sc-11397), anti-α-Tubulin (1:500; Santa Cruz Biotechnology, cat. n.: sc-5286), anti-Xbp1 (1:500; Santa Cruz Biotechnology, cat. n.: sc-7160), Ufd1 (1:500; Abcam, cat. n.: ab155003), cleaved PARP1 (1:500; Cell Signaling, cat. n.: 9544), p-eIF2a (1:500; Cell Signaling, cat. n.: 3597), ATF4 (1:500; Merck Millipore, cat. n.: ABE387), HSP90 (1.500; Enzo, cat. n.: ADI-SPA-810), HSP70 (1:500; Enzo, cat. n.: ADI-SPA-830), HSF1(1:500; Cell Signaling, cat. n.: 4356), pHSP27 (1:1000; Abcam, cat. n.: 155987), HSP27 (1:1000; Abcam, cat. n.: 109376) followed by detection by secondary antibodies: goat-anti mouse IgG-HRP (GE Healthcare), goat-anti rabbit (GE Healthcare), donkey-anti goat IgG-HRP (Santa Cruz Biotechnology, sc-2020). Bounded secondary antibodies were visualized by ELC detection reagent (Thermo Scientific) and images were recorded by imaging system equipped with CCD camera (ChemiDoc, Bio-Rad) operated by Image Lab software or developed on film (Amersham).

Immunofluorescence staining

Cells were grown in 24-well plates with 0.170mm glass bottom (In Vitro Scientific). Where indicated, the cells were pre-extracted before fixation with pre-extraction buffer (10 mM PIPES, pH 6.8, 100 mM NaCl, 1.5 mM $MgCl_2$, 300 mM sucrose, 0.5% Triton-X 100, 1mM DTT, 5 μg/ml leupeptin, 2 μg/ml aprotinin, 0.1 mM PMSF) for 20 minutes at 4°C, washed by PBS and then immediately fixed with 4% formaldehyde for 15 minutes at room temperature. Cells were stained with primary antibodies: anti-ubiquitylated conjugateed mouse FK2 antibody (1:500; Enzo, cat. n.: BML-PW8810), anti-VCP (1:500; Abcam; cat. n.: ab11433), anti-NPL4 (1:500; Novus Bio, cat. n.: NBP1-82166), HSP70 (1:100; Enzo, cat. n.: ADI-SPA-830), HSF1 (1:500; Cell Signaling, cat. n.: 4356) anti-ubiquitin lys48-specific (1:500; Merck Millipore, clone Apu2), Sumo2/3 (1:500; Abcam, cat. n.: ab3742), TDP-43 (1:300; Proteintech, cat. n.: 10782-2-AP) and appropriate Alexa Fluor 488 and 568 secondary antibodies (Invitrogen, 1:1000). Cytochrome c was stained by Alexa Fluor 555 conjugated mouse anti-cytochrome c antibody according manufacture's protocol (BD Pharmingen, cat. n.: 558700).

Microscopy, FRAP and image analysis

Samples were examined in a Zeiss Axioimager Z.1 platform equipped with the Elyra PS.1 super-resolution module for structured illumination (SIM) and the LSM780 module for CLSM. High resolution images were acquired in super-resolution mode using Zeiss Pln Apo100x/1.46 oil objective (tot. mag. 1600x) with appropriate oil (Immersol 518F). SR-SIM setup involved 5 rotations and 5 phases for each image layer and up to 7 Z-stacks (101nm) were acquired per image. CLSM setup for FRAP and life cells acquisition involved c-Apo 40x/1.2W water immersion objective. Bleaching of regions of interest (ROI) was performed using Argon 488nm laser. Lower resolution images of fixed samples were acquired using Plan Apo 63x/1.4 Oil objective (tot. mag. 1008x). FRAP and image acquisitions were performed in Zeiss Zen 11 software. For FRAP internal Zen's "Bleach" and "Regions" modules were used. Data from FRAP analysis involving multiple bleached ROI's were exported into MS-Excel and charted. Basic processing of acquired images such as contrast and brightens setting was done in Adobe Photoshop on images exported as tiff. Quantitative microscopy-based cytometry of the IF stained samples was performed using an automatic

inverted fluorescence microscope BX71 (Olympus) in the ScanR Acquisition software (Olympus), analyzed with ScanR Analysis software (Olympus).

Cell fractionation for Triton X insoluble pellets

Cells were treated as indicated, washed in cold PBS and lysed in lysis buffer (50 mM HEPES, pH 7.4, 150 mM NaCl, 2 mM MgCl2, 10% glycerol, 0.5% Triton-X100, protease inhibitor cocktail by Roche) for 10 minutes gently agitating at 4°C. Then, cells were scraped to Eppendorf tubes and kept for another 10 minutes on ice with intermittent vortexing. After that, the lysate was centrifuged at 20.000G for 10 minutes at 4°C. Insoluble fraction and supernatant, respectively, were re-suspended in 1x LSB buffer.

Isolation of microsomal fraction

After the desired treatment in cell culture, cells were washed with cold PBS and lysed (250 mM sucrose, 20 mM HEPES pH 7.4, 10 mM KCl, 1.5 mM MgCl2, 1 mM EDTA, 1 mM DTT, protease inhibitor cocktail). Lysates were homogenised by Potter-Elvejhem PTFE homogeniser and kept on ice for 20 minutes. The homogenates were subjected to serial centrifugation steps (720G and 10000G for 5 minutes both, and 100 000G for 1 hour). Pellets and supernatants from the last ultracentrifugation step were re-suspended in the 1x LSB buffer and used for WB analysis.

Immunoperoxidase staining of pre-extracted tissue sections

Frozen sections (4–5 micrometer thick) from xenograft-grown, cryopreserved tumour tissues were cut on a cryostat and placed on commercial adhesion slides (SuperFrost Plus, Menzel, Germany) and air-dried for 2 hours at room temperature. The dried sections were carefully covered with the cold extraction buffer: 50mM Tris-HCL (pH 7,5), 150mM NaCl, 1mM MgCl2, 5% glycerol, 1mM DTT, 1% Triton-X100, 1% IGEPAL, protease inhibitor cocktail (Phos Stop Easy pack, Ref: 04906837001, Roche) or cold PBS (controls) and incubated in a cold room for 20 minutes. Pre-extracted and control PBS-treated sections were gently washed 3 times in cold PBS, and fixed in 4% paraformaldehyde fixative for 15 minutes, followed by another 3 washes in PBS. Washed sections were then subject to a sensitive immunoperoxidase staining protocol, using the primary rabbit monoclonal antibody against VCP antibody (EPR3307(2)/(ab109240, Abcam, diluted: 1:10 000) and rabbit polyclonal antibody against NPLOC4 (NBP1- 82166, Novus Biologicals, diluted 1:500) and Vectastain Elite kit as secondary reagents (Vector Laboratories, USA), followed by a nickel-sulphate-enhanced diaminobenzidine reaction without nuclear counterstaining, mounted and microscopically evaluated and representative images documented by an experienced oncopathologist.

Isothermal Titration Calorimetry (ITC)

Experiments were performed at 25 °C with a Nano ITC Low Volume (TA Instruments, New Castle, DE, USA). During all measurements, injections of 2.5 µl of ligand (16 µM) was titrated into 250 µl protein (2µM) with time intervals 300 s, a stirring speed of 250 rpm. All ITC experiments were conducted with degassed buffered solutions 20 mM Hepes buffer, pH

7.3, in the presence of 1% DMSO. Purified GST-NPL4-WT and GST-NPL4-MUT proteins were used in ITC experiment.

Drug Affinity Responsive Target Stability (DARTS)

DARTS was performed according to a modified published protocol[38]. A purified WT or MUT Npl4-GST was diluted by 100 mM phosphate buffer, pH 7.4 to final concentration of 0.03 μg/μl. The proteins were treated by CuET (final concentration of 5 μM; dissolved in DMSO) for 1 hour and equal amount of DMSO was added to the solutions which served as control samples. Pronase (Sigma-Aldrich) was dissolved in TNC buffer (50mM Tris-Cl, 50mM NaCl, 10mM $CaCl_2$, pH = 7.5). The 0.025 μg of pronase was added to 50 μl of protein solution and incubated for 1 hour at 37°C. Samples without pronase served as the nondigested controls. The pronase reaction was stopped by addition of 5×SDS loading buffer; the samples were boiled to 95°C for 15 min and loaded on SDS-PAGE gel. After the SDS-PAGE the gels were silver-stained and scanned on GS-800 Calibrated Densitometer (Bio-Rad) or used for WB analysis.

20S proteasome activity

To measure proteasome activity in the cell extracts, cell lines were seeded on 100 mm petri dishes in a density of 3×10^6 cells/dish. After 24 h cells were twice washed with 2 mL of ice-cold PBS and scraped in to 1000 μl ice-cold PBS. The cells were then isolated and suspended in buffer [50 mM HEPES (pH 7.5), 150 mM NaCl, 1% Triton X-100 and PMSF 0.1 μM] and then centrifuged at 15.000 rpm for 15 min at 4 °C. The cell lysates (10 μg) were incubated with 20 μM of substrates for measurement of chymotrypsin-like, trypsin-like and caspase-like activities [Suc-LLVT-AMC, Ac-RLR-AMC and Z-LLE-AMC (Boston Biochem)] in 90 μL of assay buffer [30 mM Tris-HCl, 0.035% sodium dodecylsulfate (pH 7.4)] in the presence CuET (1 μM and 5 μM) and bortezomib (1 μM) for the exploration of proteasome inhibition, bortezomib or equivalent volume of solvent (DMSO) as a control. After 2 h of incubation at 37°C, inhibition of each proteasome activity was measured by the release of hydrolysed free AMC groups by fluorimeter at 380/460 nm (TECAN, Infinite M200PRO). To measure proteasome activity in live cells, the cells were seeded on 24-well plate in a density of 0.2×10^6 cells/well. Cell lines were treated with CuET (1 μM and 5 μM), vehicle control and 1μM bortezomib for one hour. After incubation, cells were twice washed with 0.5 mL of ice-cold PBS 1x and scraped in 100 μL ice-cold lysis buffer and then centrifuged at 15,000 rpm for 15 min at 4 °C. Subsequently, the cell extract (10 μg) was incubated with 20 μM substrates to measure chymotrypsin-like, trypsin-like and caspase-like activities in assay buffer [30 mM Tris-HCl (pH 7.4)]. After 2 hours of incubation at 37°C, inhibition of proteasome enzymatic activities was measured by the release of hydrolysed free AMC as described above.

$Ub^{(G76V)}$-GFP degradation

HeLa-Ub(G76V)-GFP-ODD-Luc cells expressing $Ub^{(G76V)}$-GFP were seeded at density 10^4 cells/well to 96-well plates. Next day the cells were treated with 4 μM MG132 for 3 hours. After that, the medium was discarded and cells were twice washed with PBS and then incubated with tested compound in the presence of 30 μg/ml cycloheximide for another 3 hours. GFP signal was acquired using ImageXpress automated microscope. For each well

four images were taken (corresponding to 200-250 cells). Cells were analysed every 30 minutes during 3 hours of treatment. Normalized GFP signal intensity was calculated using the following formula: (Test compound – Background)/(Basal GFP signal intensity – Background). Where: Test compound is defined as Mean GFP signal intensity of $Ub^{(G76V)}$-GFP-expressing cells treated with the test compound. Background is defined as background GFP signal intensity of HeLa cells. Basal GFP signal intensity is defined as mean GFP signal intensity of $Ub^{(G76V)}$-GFP-expressing cells treated with DMSO. The degradation rate constant (k) was obtained from the slope of the linear range of plotting Ln (Normalized GFP signal intensity) versus time ranging from 90 to 180 min. The percent of remaining k for each compound is calculated using the following formula: (Test compound/DMSO control) * 100.

p97 ATPase activity assay

P97 ATPase assay was performed as described previously[28]. 250 nM of p97 protein was diluted in assay buffer (50 mM Tris-HCl pH 7.4, 20 mM MgCl2, 0.5 mM DTT). Test compounds were added in DMSO (final concentration of DMSO was 5%). After 10 minutes of incubation, the reaction was started with ATP (100 μM final concentration) followed by 1 hour incubation at room temperature. The reaction was stopped by adding Biomol green solution (Enzo) and free phosphate was measured according to manufacturer instructions. Results are expressed as a percent activity of the control (well containing only DMSO).

26S proteasome activity

The Rpn11 assay is described in PubChem (AID588493). Briefly, a synthetic fluorescent labeled substrate, Ub4pepOG was used to measure Rpn11 activity. Fluorescence polarization assay was performed in a low-volume 384-well solid black plate in the presence of 1) 5 μl compound (difference concentration of 1, 10 phenathroline or CuEt) in 3% DMSO or 3% DMSO control 2) 5 μl of BioMol 26S proteasome and 3) 5μl of substrate (15 nM Ub4-pepOG). Fluorescence polarization is measured using a plate reader with excitation of 480 nm and emission of 520 nm filter set. The activity was normalized to DMSO control and fitted using dose-response equation.

Protein expression and purification

All proteins were expressed in *E. coli* BL21 (DE3) cells (Novagen). p97-His (pET28a vector) and Ufd1-His (pET28a vector) expression were induced by 1 mM IPTG (Life Technologies) at an OD600 of 0.6 for 10 hours at 22°C. NPL4 WT and MUT (pGEX-2TK) were induced by 0.4 mM IPTG at an OD600 of 0.8 overnight at 16°C. In case of p97 and UFD1, bacterial pellet was suspended in buffer (50 mM Tris-HCl pH 8.0, 300 mM NaCl, 2.5 mM MgCl2, 20 mM imidazole, 5% glycerol) and lysed by sonication and centrifuged (14000G for 20 minutes). Proteins were purified by Ni-NTA chromatography (Qiagen) according to manufacturer instructions. In case of p97, the protein was further purified by gel filtration (Superdex 200, GE Healthcare). In case of WT and MUT GST-NPL4, bacterial pellet was suspended in phosphate buffer (PBS, 0.1% Triton-X100, 300 mM NaCl) and lysed by sonication and centrifuged (14000G for 10 min). Proteins were purified by glutathione sepharose 4B (Life Technologies) according manufacturer's protocol. The proteins were further purified by gel filtration (Superdex 200, GE Healthcare).

Chemicals

CuET was prepared by direct synthesis from water solutions of diethyldithiocarbamate sodium salt and copper (II) chloride as described previously[53]. CuET for in vivo experiments was prepared equally with slight modification. The reaction between diethyldithiocarbamate sodium salt and copper (II) chloride was performed in the sterile 1% aqueous solution of bovine serum albumin. Resulting solution was directly used. The following chemicals were purchased from commercial vendors: tetraethylthiuram disulfide (disulfiram, DSF) (Sigma), sodium diethyldithiocarbamate trihydrate (Sigma), copper-D-gluconate (Sigma), bortezomib (Velcade, Janssen-Cilag International N.V.), MG132 (Sigma), DBeQ (Sigma), NMS873 (Abmole), cycloheximide (Sigma), dicoumarol (Sigma), 1,10-phenanthroline (Sigma), MLN7243 (Active Biochem).

Statistical analyses and reproducibility

For the epidemiological study, we calculated hazard ratios (HRs) and 95% confidence intervals (CIs) estimating cancer-specific mortality, based on a Cox model regressing on both propensity scores and disulfiram use, balancing baseline characteristics of ‘previous’ and ‘continuing’ users of DSF and adjusting estimated hazard ratios of cancer-specific mortality associated with DSF use[51]. The propensity scores estimates were conditional on multiple covariates, based on using logistic regression (see the Methods section: Epidemiological analyses and access to health registers for specifics of cohorts and covariates). In the Cox model, the propensity score is further included as a restricted cubic spline to model possible non-linearity’s, in addition to the categorical disulfiram use as the variable of main interest. Statistical significance of DSF use was evaluated by likelihood ratio tests, using the software R for statistical computing[52].

For evaluation of the animal studies, STATISTICA software, ver. 12 (StatSoft Inc., USA) was used to estimate the sample size. For the power of 80%, the level of significance set at 5%, 4 groups and RMSSE = 0.8, 7 mice in each group was estimated. For usage of non-parametrical statistical methods, the number of 8 mice in each group was finally planned. The differences between tumour volumes were statistically analyzed by non-parametrical Kruskal-Wallis test not requiring any assumptions according to normality and homoscedascity. To test impact of CuET treatment on AMO-1 xenografted mice survival reflected in Kaplan-Meier chart log-rank statistical test was used. For other experiments the descriptive statistics such as number of repetitions, centre value and error bars are specified in figure legends.

DATA AVAILABILITY STATEMENT

Most data generated or analysed during this study are included in this published article and its supplementary information files. Uncropped images of all gels and blots in this study can be found in Supplementary Fig. 1. Source Data for all charts are provided. Additional datasets generated during and/or analysed during the current study and relevant information are available from the corresponding authors upon reasonable request.

Extended Data

a

Cancer type	Overall			
	No [a]	HR	95 CI	p-value
Colon cancer				
Previous users	326	1.00		
Continuing users	103	0.75	0.66-0.85	0.000
No prescriptions	31,812	0.84	0.79-0.91	0.000
Prostate cancer				
Previous users	377	1.00		
Continuing users	175	0.81	0.66-0.98	0.029
No prescriptions	36,338	0.86	0.75-0.98	0.021
Breast cancer				
Previous users	408	1.00		
Continuing users	192	0.75	0.50-1.12	0.163
No prescriptions	48,106	0.62	0.49-0.78	0.000

[a] number of patients included

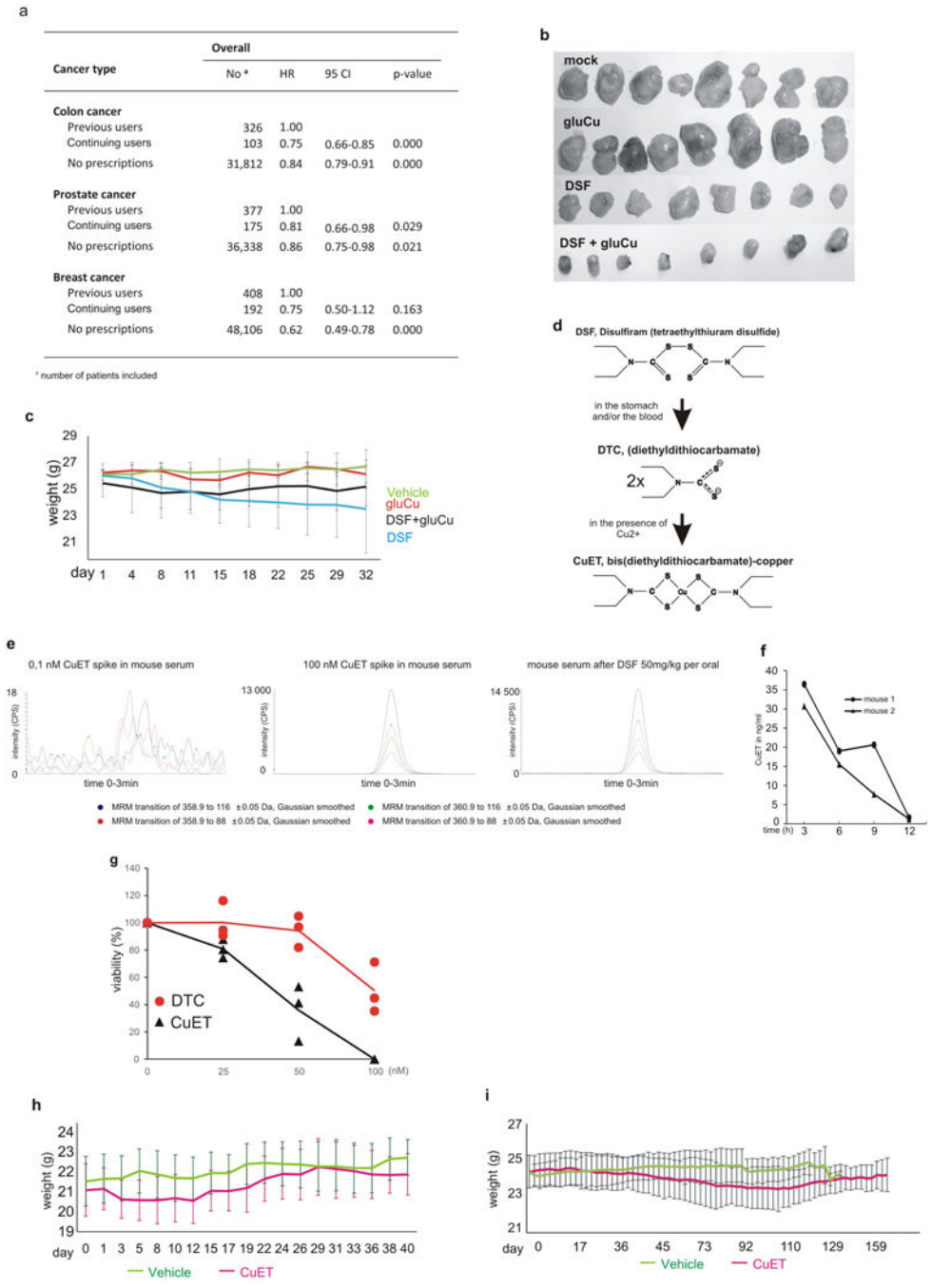

Extended Data 1. Anti-cancer effects of DSF: epidemiological and pre-clinical data

a) Summary of Hazard Ratios (HR) and 95% confidence intervals (CI) for cancer-specific mortality among Danish cancer patients comparing continuing and previous users of disulfiram (DSF) for selected types of cancer (for statistical analysis and definitions of DSF exposure categories, see Methods); **b**) Photographs of subcutaneously growing human MDA-MB-231 tumours extracted from mice at day 32; **c**) Time-course diagram of mice

weight (n=8 animals per group, mean, SD); **d**) Model of CuET formation during metabolic processing of orally administered DSF in the human body. **e**) Examples of Mass-spectrometry Spectra of CuET expressed as peaks of 4 MRM transitions in murine serum after CuET spikes, compared to orally applied DSF (50 mg/kg) (representative of two independent experiments). **f**) Pharmacokinetic analysis of CuET levels in murine serum after orally applied DSF (50 mg/kg) (mean, SD, n=2 animals for each time point). **g**) Effect of DTC and CuET on MDA-MB-231 cells analysed by colony formation assay (CFA) (3 independent experiments, means linked). **h**) Time-course diagram of weight in CuET- and vehicle-treated mice (n=10 animals per group, mean, SD); **i**) Extended time-course diagram of weight in CuET- and vehicle-treated mice (n=10 animals per group, mean, SD).

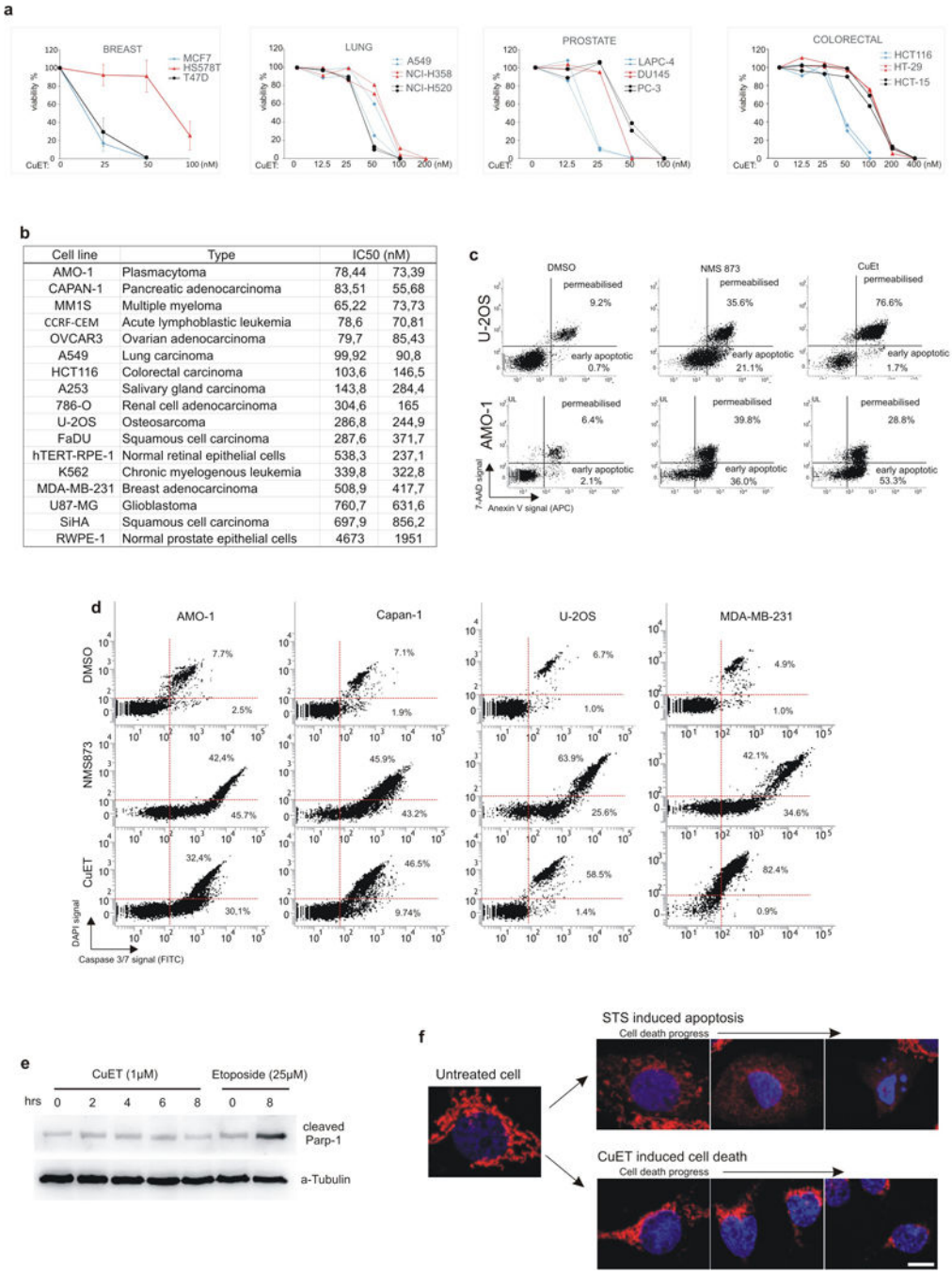

Cell line	Type	IC50 (nM)	
AMO-1	Plasmacytoma	78,44	73,39
CAPAN-1	Pancreatic adenocarcinoma	83,51	55,68
MM1S	Multiple myeloma	65,22	73,73
CCRF-CEM	Acute lymphoblastic leukemia	78,6	70,81
OVCAR3	Ovarian adenocarcinoma	79,7	85,43
A549	Lung carcinoma	99,92	90,8
HCT116	Colorectal carcinoma	103,6	146,5
A253	Salivary gland carcinoma	143,8	284,4
786-O	Renal cell adenocarcinoma	304,6	165
U-2OS	Osteosarcoma	286,8	244,9
FaDU	Squamous cell carcinoma	287,6	371,7
hTERT-RPE-1	Normal retinal epithelial cells	538,3	237,1
K562	Chronic myelogenous leukemia	339,8	322,8
MDA-MB-231	Breast adenocarcinoma	508,9	417,7
U87-MG	Glioblastoma	760,7	631,6
SiHA	Squamous cell carcinoma	697,9	856,2
RWPE-1	Normal prostate epithelial cells	4673	1951

Extended Data Figure 2. CuET as the major anticancer metabolite of DSF

a) CuET cytotoxicity measured by a Colony formation assay (CFA) in human cell lines derived from breast (mean and SD from 3 independent experiments), lung, colon and prostate carcinomas (presented 2 independent biological experiments for each cell line); **b**) IC50 values from two independent biological experiments documenting differential CuET-induced cytotoxicity across a panel of cancer and non-cancerous cell lines (48h treatment); **c**) Analysis of AnexinV signal in AMO-1 cells exposed to toxic doses of NMS873 (5μM, 16h) or CuET (100nM, 16h) and in U-2OS cell exposed to toxic doses of NMS873 (10μM,

16h) or CuET (1μM, 16h); **d**) Analysis of Caspase 3/7 activity in selected cell lines after apoptosis induction by NMS873 (AMO-1: 6h, 5μM, Capan1: 16h, 10μM, U-2OS: 16h, 10μM, MDA-MB-231: 24h,10μM) or CuET (AMO-1: 16h, 100nM, Capan1: 16h, 250nM, U-2OS: 16h, 1μM, MDA-MB-231: 24h, 1 μM) **e**) Absence of cleaved Parp1 after toxic dose of CuET in U-2OS cells, compared to etoposide treatment as a positive control; **f**) Analysis of Cytochrome C (in red) release from mitochondria in U-2OS cells during cell death induced either by the positive control staurosporin (STS, 1μM) compared to cell death induced by CuET (1μM) (blue=DAPI signal). Panels c-f are representative of two independent biological experiments.

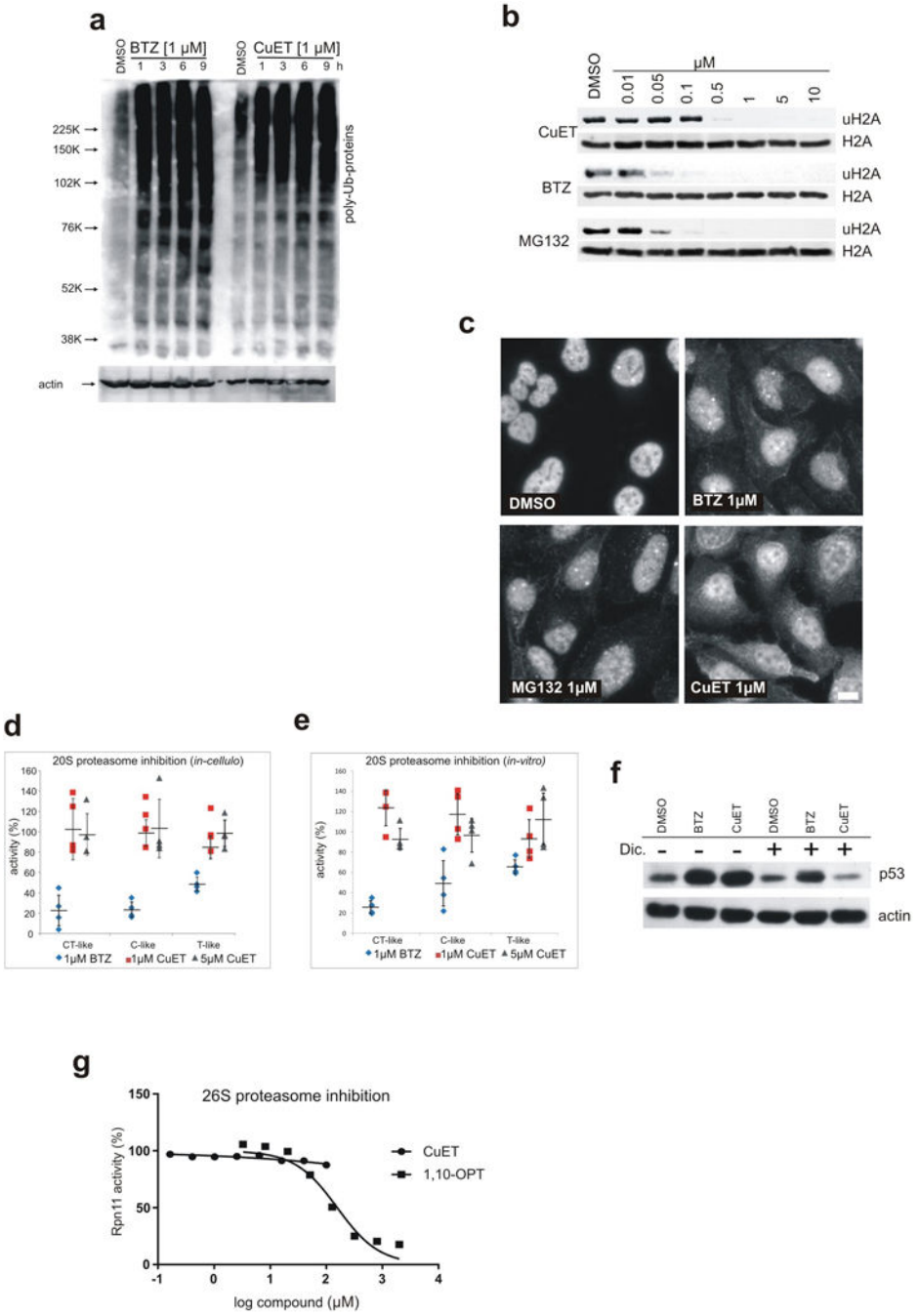

Extended Data Figure 3. CuET-induced proteasome inhibition-like response is not due to proteasome inhibition

a) Kinetics of poly-Ub-protein accumulation in U-2OS cells treated with CuET or the proteasome inhibitor BTZ; **b**) CuET treatment (1,5h) induces rapid deubiquitylation of ubiquitylated histone H2A (uH2A) similarly to proteasome inhibitors BTZ or MG132 (U-2OS cells); **c**) CuET treatment (1,5h) induces rapid cytoplasmic accumulation of poly-ubiquitylated proteins (FK2 antibody staining, U-2OS cells); analogous to BTZ and MG132; **d**) 20S proteasome activity is not inhibited by CuET as examined in live MDA-MB-231

cells or **e**) in lysates from MDA-MB-231 cells (mean and SD from 4 independent experiments); **f**) CuET treatment (1μM, 6h) does not cause accumulation of p53 in the presence of Dicoumarol (300 μM) in MCF7 cells; **g**) In-vitro 26S proteasome function measured as Rpn11 deubiquitylation activity, is not inhibited by CuET; 1,10 phenantroline (1,10-OPT) served as a positive control (representative of three independent experiments). Panels a-c, f are representative of two independent experiments.

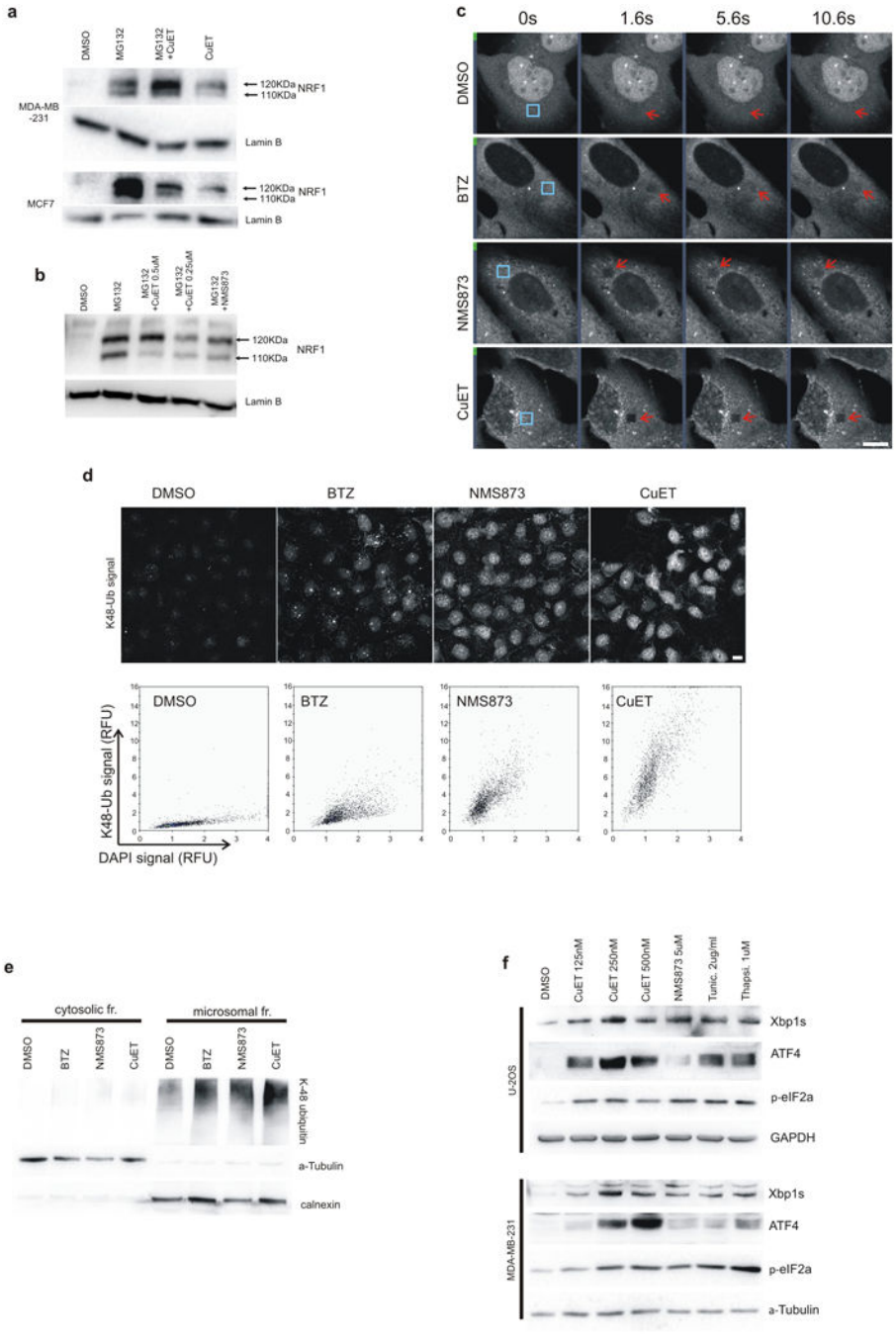

Extended Data Figure 4. CuET inhibits the p97 pathway and induces cellular unfolded protein response (UPR)

a) Proteasome inhibitor MG132-treated cells (5μM, 6h) accumulate both forms of NRF1 (120- and 110-KDa bands, upper and lower arrows, respectively) while CuET-treated cells (1μM, 6h) accumulate only the non-cleaved 120-KDa form; **b**) Inhibition of the NRF1 cleavage process (appearance of the lower band) by CuET and NMS873 (a p97 inhibitor; 5μM) in mouse NIH3T3 cells co-treated with the proteasome inhibitor MG132 (5μM for 6h); **c**) Time-course example images from a FRAP experiment the quantitative analysis of which is shown in Fig. 2g (U-2OS cells, blue boxes mark areas before bleaching, arrows after bleaching); **d**) U-2OS cells pre-extracted by TritonX and stained for K-48-polyUb. The Ab signal intensities for cells treated with DMSO, BTZ (1μM), NMS873 (10μM) and CuET (1μM) are analysed by microscopy-based cytometry and plotted below; **e**) Western blot analysis of accumulated poly-Ub proteins in ultracentrifugation-separated microsomal fraction from U-2OS cells treated by mock, CuET (1μM), NMS873 (10μM) or BTZ (1μM) for 3h; **f**) UPR in U-2OS and MDA-MB-231 cell lines induced by 6-h treatment with CuET (various concentrations) or positive controls (NMS873 5μM, tunicamycin 2μg/ml, thapsigargin 1μM) manifested by increased levels of Xbp1s, ATF4 and p-eIF2a. Panels a-f are representative of two independent experiments.

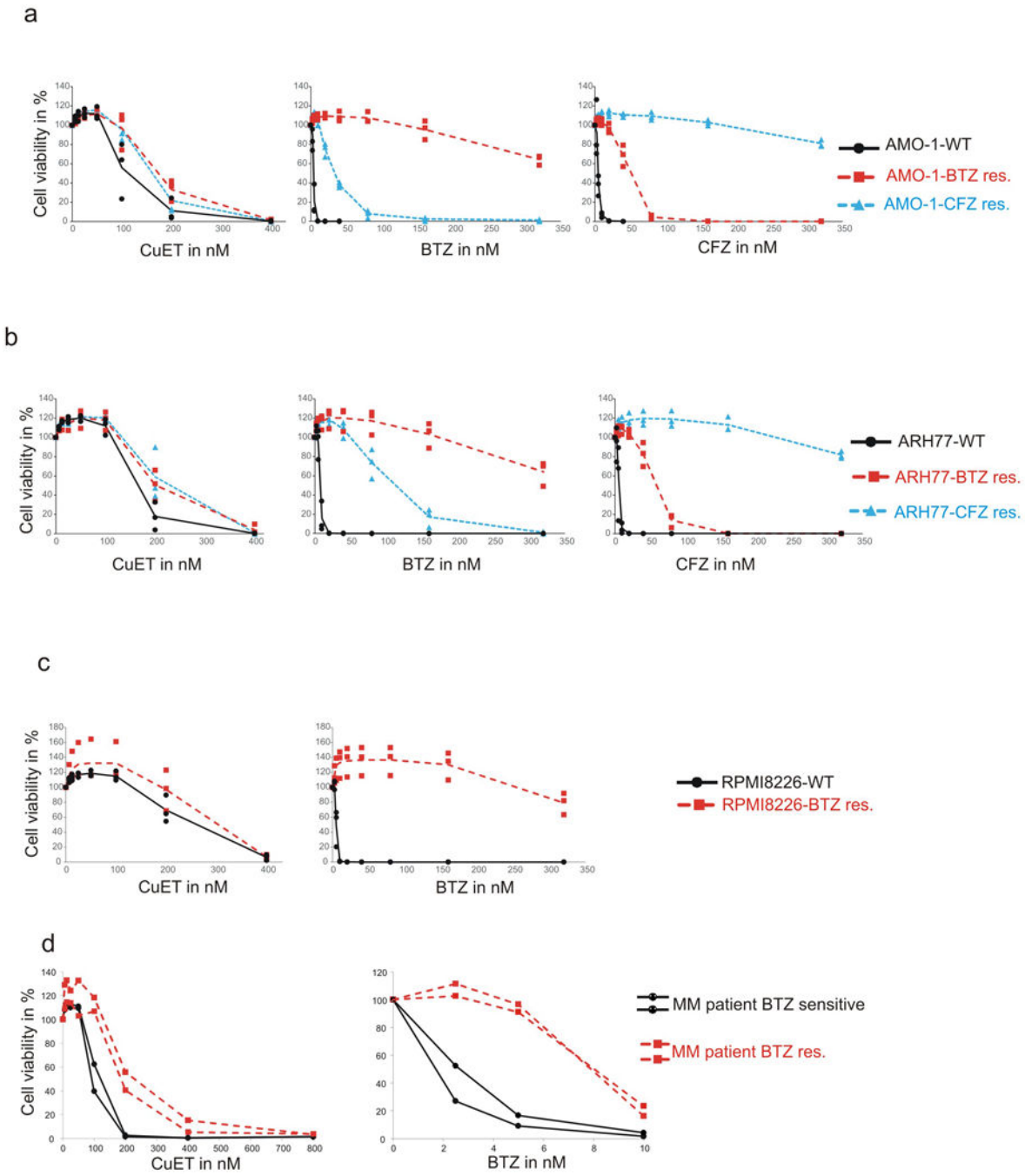

Extended Data Figure 5. CuET kills bortezomib-resistant cells

a) Bortezomib/Carfilzomib (BTZres/CFZres)-adapted and non-adapted AMO-1 human myeloma cells are similarly sensitive to treatment with CuET; **b**) Bortezomib/Carfilzomib (BTZres/CFZres)-adapted and non-adapted ARH77 human plasmocytoma cells are similarly sensitive to treatment with CuET; **c**) Bortezomib (BTZres)-adapted and non-adapted RPMI8226 human myeloma cells are similarly sensitive to treatment with CuET; **d**) Human myeloma cells derived from a BTZ-resistant patient show CuET sensitivity comparable with

myeloma cells derived from a BTZ-sensitive patient. The charts in (ac) show three independent experiments (means linked), panel (d) shows two independent experiments.

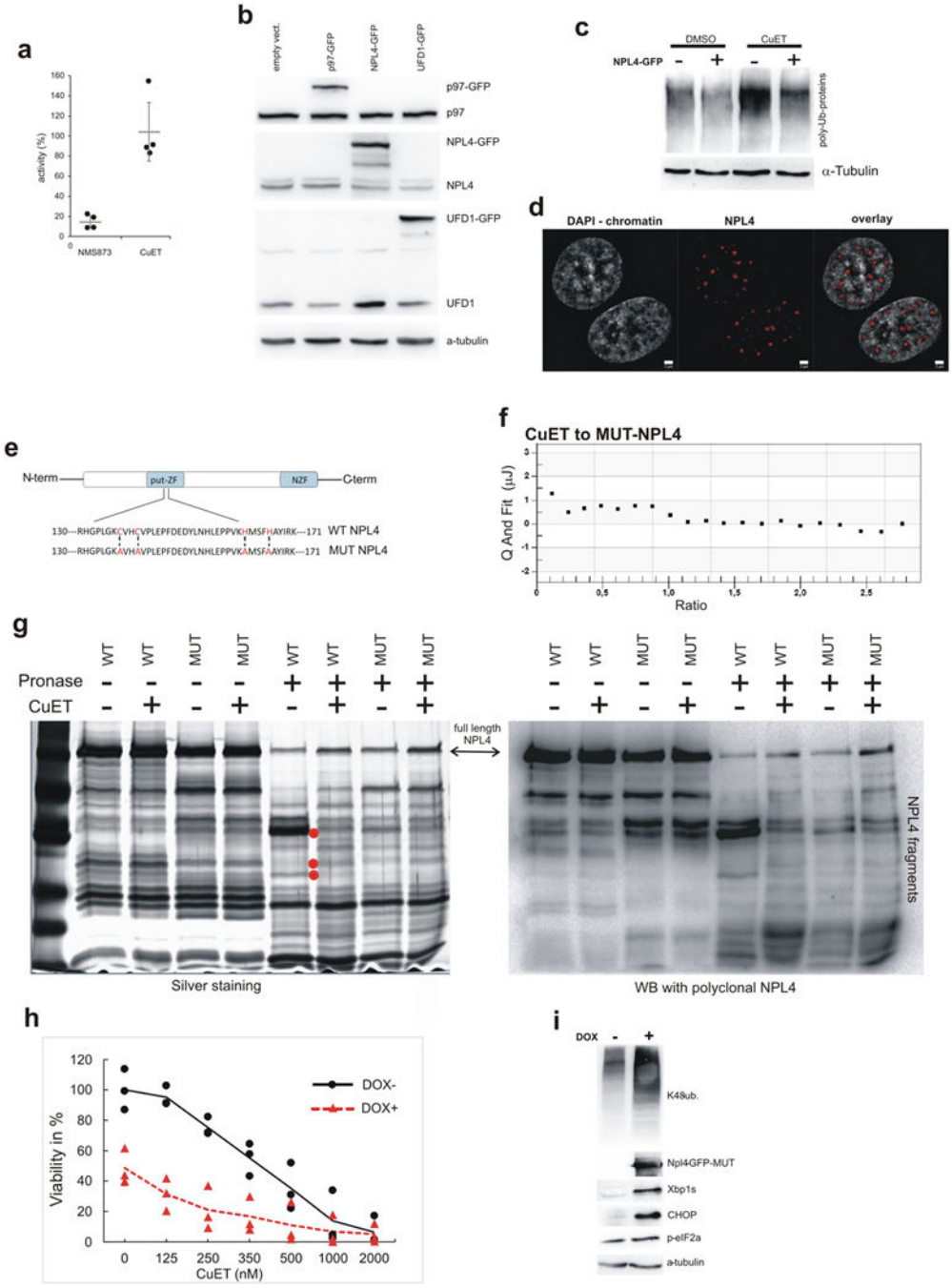

Extended Data Figure 6. CuET targets NPL4, causing NPL4's immobilization and nuclear clustering

a) CuET (1µM) does not inhibit ATPase activity of p97; NMS873 (5µM) was used as a positive control (mean, SD from 4 independent experiments); **b**) Western blotting analysis documenting levels of ectopic p97-GFP, NPL4-GFP and UFD1-GFP in stable U-2OS-derived cell lines used for the CuET-treatment rescue and cluster formation experiments; **c**)

Ectopic expression of NPL4-GFP alleviates CuET-induced (125nM, 4h) accumulation of poly-Ub proteins in U-2OS cells; **d**) Distribution of NPL4 nuclear clusters relative to chromatin in cells treated by CuET (1μM, 2h) (Scale bar = 2 micrometres); **e**) Schematic representation of site-directed mutagenesis within the amino acid sequence of the putative zinc finger domain of NPL4; **f**) Isothermal calorimetry curve documenting the lack of CuET binding to purified MUT-NPL4 protein; **g**) DARTS analysis of recombinant NPL4 proteins: differential pronase-mediated proteolysis after CuET addition is apparent for WT-NPL4 but not for MUT-NPL4; detected by either Silver-stained SDS-PAGE (the most prominent differential bands are marked by red dots) or by blotting with an anti-NPL4 polyclonal antibody; **h**) Viability of cells expressing a doxycycline-inducible MUT-NPL4-GFP, treated with CuET for 48 h (3 independent experiments, means are linked); **i**) Accumulation of K48-ubiquitinated proteins and activation of UPR in cells expressing the doxycycline-inducible MUT-NPL4-GFP. Panels b-d, f, g and i are representative of two independent experiments.

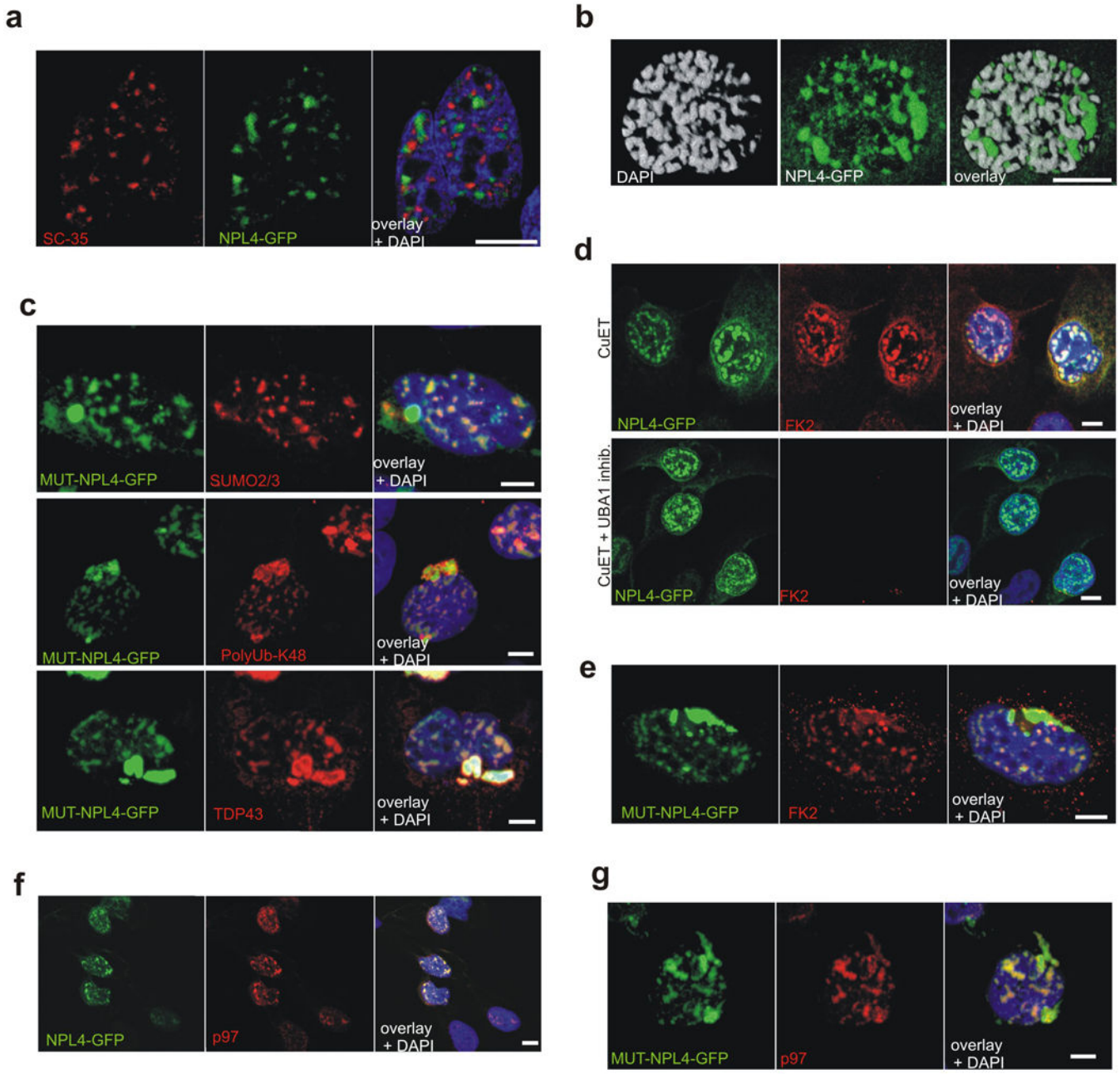

Extended Data Figure 7. Immobilized NPL4 forms insoluble protein aggregates

a) NPL4-GFP aggregates induced by CuET treatment (1μM for 3h) do not co-localize with nuclear speckles (stained by SC-35 antibody) or nucleoli (visible as DAPI-negative nuclear signal); **b**) NPL4-GFP nuclear aggregates induced by CuET (1μM, 3h) are excluded from chromatin in early prometaphase U-2OS cells; **c**) Co-localization of spontaneous MUT-NPL4-GFP aggregates with Sumo 2/3, K-48 polyubiquitin and TDP43 (U-2OS cells, pre-extracted); **d**) NPL4-GFP aggregates are formed independently of ubiquitylations, as documented on CuET (1μM, 3h) treated cells pre-treated with a chemical UBA1 inhibitor (MLN7243, 10 μM for 1h); The lack of the cellular FK2 staining for ubiquitylated proteins validates the efficacy of the MLN7243 inhibitor; **e**) Co-localization of FK2 signal with the

spontaneous MUT-NPL4-GFP aggregates (U-2OS cells, pre-extracted); **f**) Analysis of p97 in CuET-induced (1μM for 3h) NPL4-GFP aggregates (U-2OS cells, pre-extracted); **g**) Analysis of p97 in spontaneous MUT-NPL4-GFP aggregates (U-2OS cells, pre-extracted). Panels a-g are representative of two independent biological experiments.

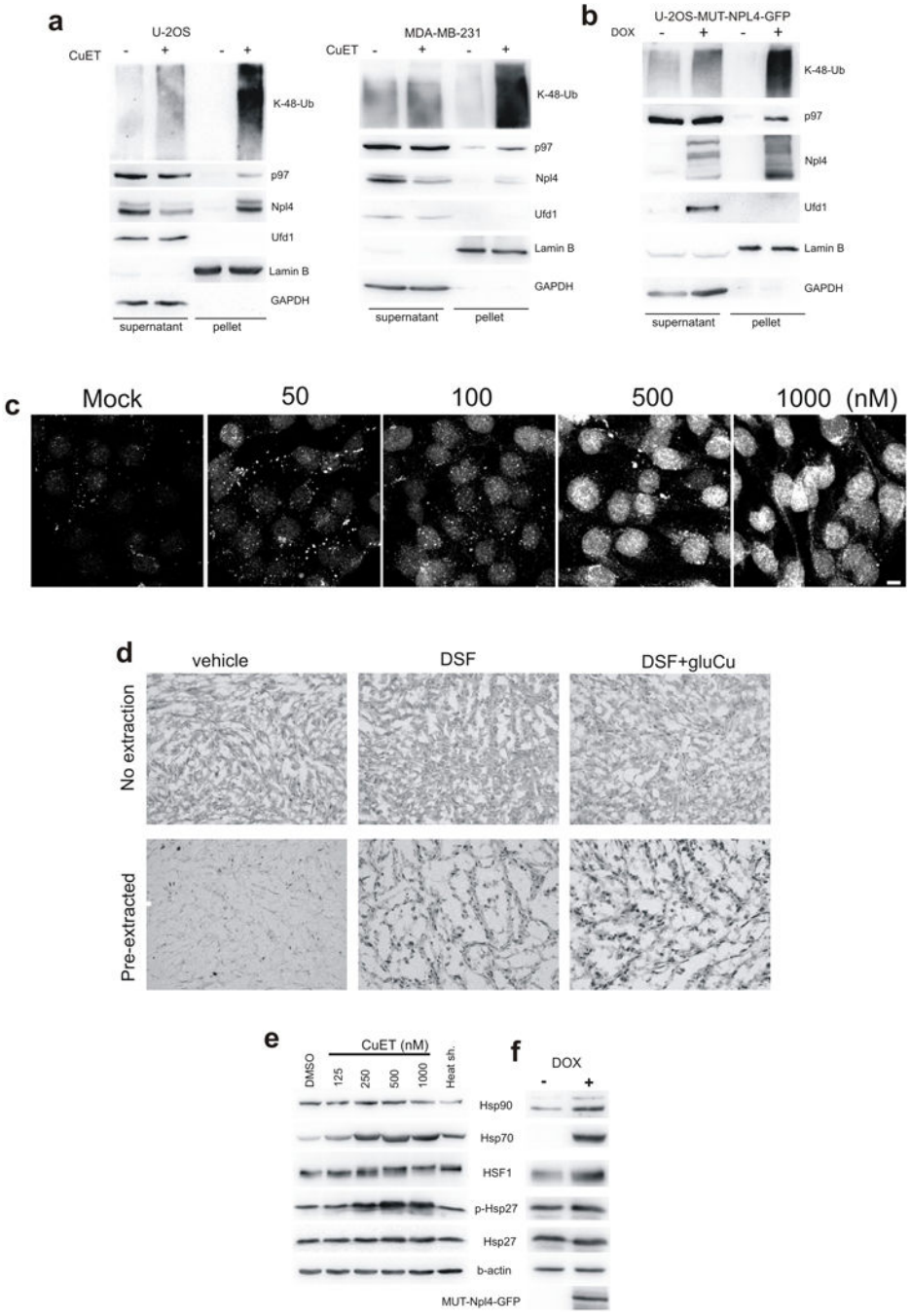

Extended Data Figure 8. NPL4 aggregation immobilizes the p97 binding partner and induces global cellular heat shock response (HSR)

a) Immobilization of selected proteins in Triton X100-resistant pellet fractions of CuET-treated (1μM, 3h) U-2OS cells; **b**) Immobilization of selected proteins in Triton X100-

resistant pellet fractions from U-2OS cells expressing doxycycline-inducible MUT-NPL4-GFP (48h after induction); **c**) CuET dose-dependent immobilization of p97 in Triton X100-pre-extracted MDA-MB-231 cells (3h); **d**) Immunohistochemical staining documenting non-extractable p97 in MDA-MB-231 xenografts from mice treated by DSF or DSF+gluCu, compared to vehicle; **e**) HSR after CuET (8h treatment) manifested by various HSR markers detected by Western blotting of U-2OS cell extracts; **f**) HSR markers in U-2OS cells expressing doxycycline-inducible MUT-NPL4-GFP (24h after induction). Panels a-f are representative of two independent biological experiments.

Supplementary Material

Refer to Web version on PubMed Central for supplementary material.

Acknowledgments

We thank Jiří Škvor, Marie Zadinová, Jiří Večerka and Dalibor Doležal for help with animal experiments, Jana Vrbkova for statistical analysis, David Fridecky and Tomas Adam for help with HPLC, Iva Protivankova and Maria Grønvig Nielsen for technical assistance. This work was supported by grants from the Kellner Family Foundation, Czech National Program of Sustainability, Grant Agency of the Czech Republic, MEYS CR project Czech-BioImaging, the Czech Health Research Council, of the Danish Cancer Society, the Danish National Research Foundation (project CARD), the Danish Council for Independent Research, the Novo Nordisk Foundation, the Czech Cancer League, the Swedish Research Council, Cancerfonden of Sweden, the European Commission (EATRIS), the Czech Ministry of Education, youth and sports (OPVKCZ), Cancer Research Czech Republic and the Howard Hughes Medical Institute.

Reference List

1. Collins FS. Mining for therapeutic gold. Nat Rev Drug Discov. 2011; 10(6):397. [PubMed: 21629277]
2. Pantziarka P, et al. The Repurposing Drugs in Oncology (ReDO) Project. Ecancermedicalscience. 2014; 8:442. [PubMed: 25075216]
3. Iljin K, et al. High-throughput cell-based screening of 4910 known drugs and drug-like small molecules identifies disulfiram as an inhibitor of prostate cancer cell growth. Clin Cancer Res. 2009; 15(19):6070–6078. [PubMed: 19789329]
4. Cvek B. Nonprofit drugs as the salvation of the world's healthcare systems: the case of Antabuse (disulfiram). Drug Discov Today. 2012; 17(9–10):409–412. [PubMed: 22192884]
5. Shen ML, et al. Determination of in vivo adducts of disulfiram with mitochondrial aldehyde dehydrogenase. Biochem Pharmacol. 2001; 61(5):537–545. [PubMed: 11239496]
6. Chen D, et al. Disulfiram, a clinically used anti-alcoholism drug and copper-binding agent, induces apoptotic cell death in breast cancer cultures and xenografts via inhibition of the proteasome activity. Cancer Res. 2006; 66(21):10425–10433. [PubMed: 17079463]
7. Zha J, et al. Disulfiram targeting lymphoid malignant cell lines via ROS-JNK activation as well as Nrf2 and NF-kB pathway inhibition. J Transl Med. 2014; 12:163. [PubMed: 24915933]
8. Safi R, et al. Copper signaling axis as a target for prostate cancer therapeutics. Cancer Res. 2014; 74(20):5819–5831. [PubMed: 25320179]
9. Liu P, et al. Liposome encapsulated Disulfiram inhibits NFkappaB pathway and targets breast cancer stem cells in vitro and in vivo. Oncotarget. 2014; 5(17):7471–7485. [PubMed: 25277186]
10. Dufour P, et al. Sodium dithiocarb as adjuvant immunotherapy for high risk breast cancer: a randomized study. Biotherapy. 1993; 6(1):9–12. [PubMed: 8389572]
11. Yip NC, et al. Disulfiram modulated ROS-MAPK and NFkappaB pathways and targeted breast cancer cells with cancer stem cell-like properties. Br J Cancer. 2011; 104(10):1564–1574. [PubMed: 21487404]

12. Lovborg H, et al. Inhibition of proteasome activity, nuclear factor-KappaB translocation and cell survival by the antialcoholism drug disulfiram. Int J Cancer. 2006; 118(6):1577–1780. [PubMed: 16206267]
13. Allensworth JL, et al. Disulfiram (DSF) acts as a copper ionophore to induce copper-dependent oxidative stress and mediate anti-tumor efficacy in inflammatory breast cancer. Mol Oncol. 2015; 9(6):1155–1168. [PubMed: 25769405]
14. Nechushtan H, et al. A phase IIb trial assessing the addition of disulfiram to chemotherapy for the treatment of metastatic non-small cell lung cancer. Oncologist. 2015; 20(4):366–367. [PubMed: 25777347]
15. Jin M, et al. Alcohol drinking and all cancer mortality: a meta-analysis. Ann Oncol. 2013; 24(3): 807–16. [PubMed: 23104725]
16. Li Y, et al. Copper improves the anti-angiogenic activity of disulfiram through the EGFR/Src/VEGF pathway in gliomas. Cancer Lett. 2015; 369(1):86–96. [PubMed: 26254539]
17. Suzuki Y, et al. The origin of an EPR signal observed in dithiocarbamate-loaded tissues. Copper(II)-dithiocarbamate complexes account for the narrow hyperfine lines. Biochim Biophys Acta. 1997; 1335(3):242–245. [PubMed: 9202186]
18. Kepp O, et al. Cell death assays for drug discovery. Nat Rev Drug Discov. 2011; 10(3):221–237. [PubMed: 21358741]
19. Doil C, et al. RNF168 binds and amplifies ubiquitin conjugates on damaged chromosomes to allow accumulation of repair proteins. Cell. 2009; 136(3):435–446. [PubMed: 19203579]
20. Li JM, et al. The p97-UFD1L-NPL4 protein complex mediates cytokine-induced IkappaBalpha proteolysis. Mol Cell Biol. 2014; 34(3):335–347. [PubMed: 24248593]
21. Chou TF, Deshaies RJ. Quantitative cell-based protein degradation assays to identify and classify drugs that target the ubiquitin-proteasome system. J Biol Chem. 2011; 286(19):16546–16554. [PubMed: 21343295]
22. Kisselev AF, Goldberg AL. Monitoring activity and inhibition of 26S proteasomes with fluorogenic peptide substrates. Methods Enzymol. 2005; 398:364–378. [PubMed: 16275343]
23. Asher G, et al. Regulation of p53 stability and p53-dependent apoptosis by NADH quinone oxidoreductase 1. Proc Natl Acad Sci U S A. 2001; 98(3):1188–1193. [PubMed: 11158615]
24. Asher G, et al. A mechanism of ubiquitin-independent proteasomal degradation of the tumor suppressors p53 and p73. Genes Dev. 2005; 19(3):316–321. [PubMed: 15687255]
25. Verma R, et al. Role of Rpn11 metalloprotease in deubiquitination and degradation by the 26S proteasome. Science. 2002; 298(5593):611–615. [PubMed: 12183636]
26. Dai RM, Li CC. Valosin-containing protein is a multi-ubiquitin chain-targeting factor required in ubiquitin-proteasome degradation. Nat Cell Biol. 2001; 3(8):740–744. [PubMed: 11483959]
27. Alexandru G, et al. UBXD7 binds multiple ubiquitin ligases and implicates p97 in HIF1alpha turnover. Cell. 2008; 134(5):804–816. [PubMed: 18775313]
28. Chou TF, et al. Reversible inhibitor of p97, DBeQ, impairs both ubiquitin-dependent and autophagic protein clearance pathways. Proc Natl Acad Sci U S A. 2011; 108(12):4834–4839. [PubMed: 21383145]
29. Riemer A, et al. The p97-Ufd1-Npl4 ATPase complex ensures robustness of the G2/M checkpoint by facilitating CDC25A degradation. Cell Cycle. 2014; 13(6):919–927. [PubMed: 24429874]
30. Radhakrishnan SK, den Besten W, Deshaies RJ. p97-dependent retrotranslocation and proteolytic processing govern formation of active Nrf1 upon proteasome inhibition. Elife. 2014; 3:e01856. [PubMed: 24448410]
31. Meyer H, Bug M, Bremer S. Emerging functions of the VCP/p97 AAA-ATPase in the ubiquitin system. Nat Cell Biol. 2012; 14(2):117–123. [PubMed: 22298039]
32. Magnaghi P, et al. Covalent and allosteric inhibitors of the ATPase VCP/p97 induce cancer cell death. Nat Chem Biol. 2013; 9(9):548–556. [PubMed: 23892893]
33. Samali A, et al. Methods for monitoring endoplasmic reticulum stress and the unfolded protein response. Int J Cell Biol. 2010; 2010:830307. [PubMed: 20169136]

34. Auner HW, et al. Combined inhibition of p97 and the proteasome causes lethal disruption of the secretory apparatus in multiple myeloma cells. PLoS One. 2013; 8(9):e74415. [PubMed: 24069311]
35. Soriano GP, et al. Proteasome inhibitor-adapted myeloma cells are largely independent from proteasome activity and show complex proteomic changes, in particular in redox and energy metabolism. Leukemia. 2016; 30(11):2198–2207. [PubMed: 27118406]
36. Lass A, et al. Analysis of Npl4 deletion mutants in mammalian cells unravels new Ufd1-interacting motifs and suggests a regulatory role of Npl4 in ERAD. Exp Cell Res. 2008; 314(14):2715–2723. [PubMed: 18586029]
37. Vorackova I, et al. Purification of proteins containing zinc finger domains using immobilized metal ion affinity chromatography. Protein Expr Purif. 2011; 79(1):88–95. [PubMed: 21600288]
38. Holdgate G, et al. Biophysical methods in drug discovery from small molecule to pharmaceutical. Methods Mol Biol. 2013; 1008:327–355. [PubMed: 23729258]
39. Lomenick B, et al. Target identification using drug affinity responsive target stability (DARTS). Proc Natl Acad Sci U S A. 2009; 106(51):21984–21989. [PubMed: 19995983]
40. Becker LA, et al. Therapeutic reduction of ataxin-2 extends lifespan and reduces pathology in TDP-43 mice. Nature. 2017; 544(7650):367–371. [PubMed: 28405022]
41. Guo L, et al. A cellular system that degrades misfolded proteins and protects against neurodegeneration. Mol Cell. 2014; 55(1):15–30. [PubMed: 24882209]
42. Kim YE, et al. Molecular chaperone functions in protein folding and proteostasis. Annu Rev Biochem. 2013; 82:323–355. [PubMed: 23746257]
43. Dai C, Sampson SB. HSF1: Guardian of Proteostasis in Cancer. Trends Cell Biol. 2016; 26(1):17–28. [PubMed: 26597576]
44. Cvek B. Targeting malignancies with disulfiram (Antabuse): multidrug resistance, angiogenesis, and proteasome. Curr Cancer Drug Targets. 2011; 11(3):332–337. [PubMed: 21247389]
45. Deshaies RJ. Proteotoxic crisis, the ubiquitin-proteasome system, and cancer therapy. BMC Biol. 2014; 12:94. [PubMed: 25385277]
46. Anderson DJ, et al. Targeting the AAA ATPase p97 as an Approach to Treat Cancer through Disruption of Protein Homeostasis. Cancer Cell. 2015; 28(5):653–665. [PubMed: 26555175]
47. Cui Y, et al. High expression of valosin-containing protein predicts poor prognosis in patients with breast carcinoma. Tumour Biol. 2015; 36(12):9919–9927. [PubMed: 26168958]
48. Yamamoto S, et al. Expression of valosin-containing protein in colorectal carcinomas as a predictor for disease recurrence and prognosis. Clin Cancer Res. 2004; 10(2):651–657. [PubMed: 14760088]
49. Tsujimoto Y, et al. Elevated expression of valosin-containing protein (p97) is associated with poor prognosis of prostate cancer. Clin Cancer Res. 2004; 10(9):3007–3012. [PubMed: 15131036]
50. Thygesen LC, et al. Introduction to Danish (nationwide) registers on health and social issues: structure, access, legislation, and archiving. Scand J Public Health. 2011; 39(7 Suppl):12–16. [PubMed: 21898916]
51. Rosenbaum PR, et al. The central role of the propensity score in observational studies for causal effects. Biometrika. 1983; 70(1):41–55.
52. R Core Team. A language and environment for statistical computing. R Foundation for Statistical Computing; Vienna, Austria: URL https://www.R-project.org/
53. Cvek B, et al. Ni(II), Cu(II), and Zn(II) diethyldithiocarbamate complexes show various activities against the proteasome in breast cancer cells. J Med Chem. 2008; 51(20):6256–6258. [PubMed: 18816109]

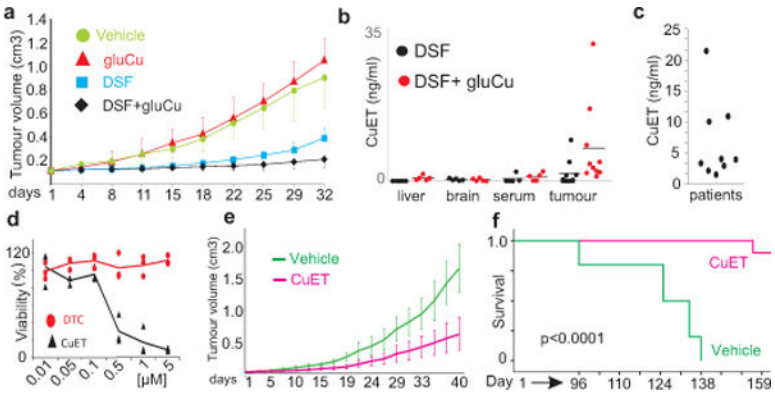

Figure 1. Tumour-suppressing effects of DSF and CuET

a) Effects of per-oral DSF and gluCu on subcutaneous growth of MDA-MB-231 tumours (n=8 mice/group, mean, SD); **b**) CuET levels in mouse tumours and tissues (n=5 tissues, n=10 tumours, mean); **c**) CuET levels in human plasma after DSF treatment (n=9 patients); **d**) Toxicity of DTC and CuET in MDA-MB-231 cells (24h, 3 experiments, means linked); **e**) Effect of CuET on subcutaneous growth of MDA-MB-231 tumours in mice (n=20 tumours, mean, SD); **f**) Survival of CuET- *vs* vehicle-treated mice with implanted AMO-1 xenografts (n=10 animals/group, mean, SD, log-rank test).

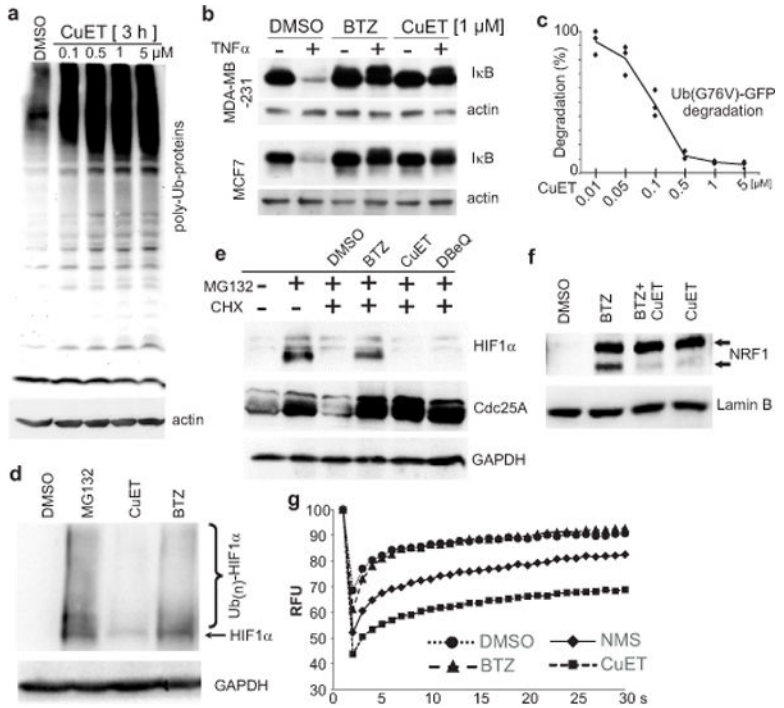

Figure 2. CuET inhibits p97 segregase-dependent protein degradation

a) CuET causes accumulation of poly-ubiquitylated proteins (MCF7 cells); **b**) TNFα-induced IκB degradation is compromised after 1-h treatment with CuET or BTZ; **c**) Dose-dependent inhibition of Ub-(G76V)-GFP degradation by CuET (3 h, HeLa cells, 3 experiments, means linked); **d**) HIF1α levels after 2-h treatments with MG132 (5μM), CuET (1μM), BTZ (1μM) (HeLa cells). **e**) Differential impact of BTZ (1μM), CuET (1μM) and DBeQ (10μM) on Cdc25A *vs* HIF1α in MG132-pretreated (4h, 5μM), cycloheximide (1h, 50μg/ml)-exposed HeLa cells (see Methods); **f**) BTZ (8h, 1μM) induces NRF1 120KDa (upper arrow) and 110KDa (lower arrow) forms; while CuET (8h, 0.5μM) only the non-cleaved 120KDa form (NIH3T3 cells); **g**) FRAP quantification in U-2OS-Ub-GFP cells: slower mobility of accumulated cytoplasmic GFP-Ub after 2h pre-treatment with NMS873 (10μM), CuET (1μM) or BTZ (1μM) (relative mean signal of the bleached region from 12 cells per treatment). Panels a, b, d-g are representative of two independent biological experiments.

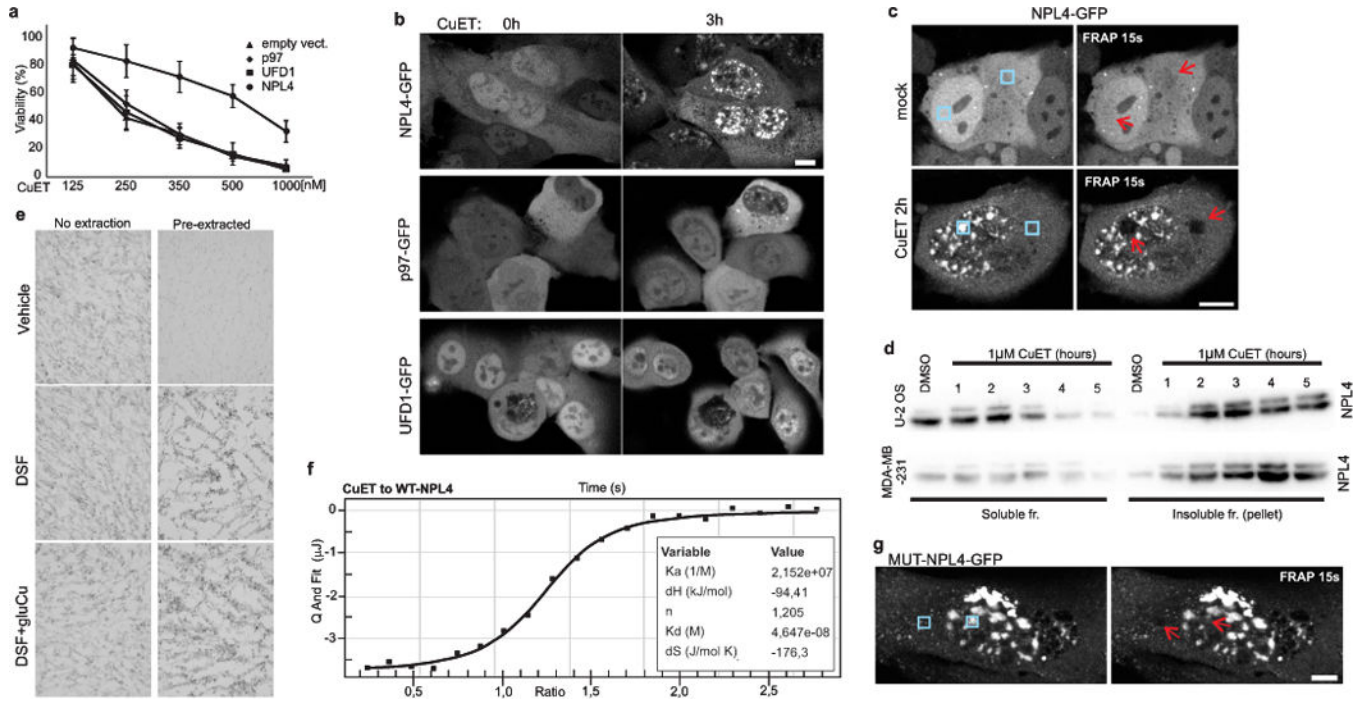

Figure 3. CuET binds and immobilizes NPL4

a) Ectopic NPL4-GFP, but not p97-GFP or UFD1-GFP rescues CuET toxicity (24h, U-2OS cells, mean, SD, 3 experiments); **b**) CuET (1μM) induces intranuclear clustering of NPL4-GFP, but not p97-GFP or UFD1-GFP; **c**) CuET(1μM, 2h)-induced immobilization of NPL4-GFP (FRAP, U-2OS cells, blue boxes: areas before bleaching, arrows: after bleaching); **d**) NPL4 enrichment in TritonX100-insoluble fractions after CuET (1μM) treatment. **e**) Immunohistochemistry highlights non-extractable NPL4: MDA-MB-231 tumours from mice treated by DSF or DSF+gluCu; **f**) Isothermal calorimetry: CuET binds to purified WT-NPL4; **g**) Spontaneous intranuclear clustering and immobilization of MUT-NPL4-GFP (FRAP, U-2OS cells, blue boxes: areas before bleaching, arrows: after bleaching). Scale bars=10μm. Panels b-g are representative of two independent experiments.

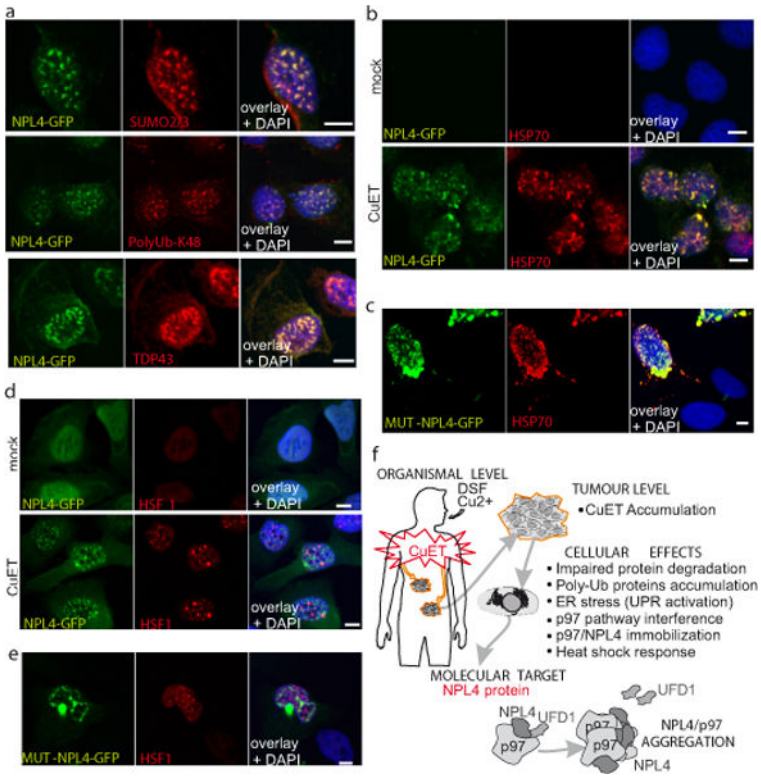

Figure 4. NPL4 protein aggregation triggers HSR

a) NPL4-GFP co-localizes with Sumo2/3, K-48 poly-Ub and TDP43 (U-2OS cells, CuET 1μM, 3h, pre-extracted); **b**) NPL4-GFP co-localizes with HSP70 in mock- and CuET-treated U-2OS cells (1μM, 3h, pre-extracted); **c**) MUT-NPL4-GFP co-localizes with HSP70 (U-2OS cells, pre-extracted); **d**) CuET-induced HSF1 stress bodies (1 μM, 3h, U-2OS-NPL4-GFP cells); **e**) HSF1 stress bodies in U-2OS cells expressing MUT-NPL4-GFP; **f**) Model of DSF anticancer activity in patients. All scale bars=10μm. Panels a-e are representative of two independent experiments.

Table 1

Cancer-specific mortality associated with DSF use among Danish cancer patients.

	Overall				Localised stage				Non-localised stage				Unknown stage			
Cancer type	**No** [a]	**HR**	**95 CI**	**p-value**	**No** [a]	**HR**	**95 CI**	**p-value**	**No** [a]	**HR**	**95 CI**	**p-value**	**No** [a]	**HR**	**95 CI**	**p–value**
Any cancer [b]																
Previous users	3,038	1.00			1,429	1.00			1,054	1.00			555	1.00		
Continuing users	1,177	0.66	0.58–0.76	0.000	602	0.69	0.64–0.74	0.000	355	0.71	0.59–0.87	0.001	220	0.65	0.57–0.75	0.000
No prescriptions	236,950	0.68	0.64–0.73	0.000	113,354	0.59	0.57–0.61	0.000	73,933	0.80	0.73–0.88	0.000	49,663	0.66	0.62–0.71	0.000

[a] number of patients included

[b] except cancers of the liver and kidney

Hazard ratios (HR) and 95% confidence intervals (CI) comparing continuing and previous users of DSF, relative to the time of their cancer diagnosis. For definitions of DSF exposure categories, statistics and clinical stages, see Methods.